공학박사 학위논문

Autostereoscopic Three-dimensional Imaging Methods using Holographic Recording Techniques on Photopolymer

포토폴리머 상의 홀로그래픽 기록 기술을 이용한 무안경식 삼차원 이미징 방법

2014년 8월

서울대학교 대학원

전기컴퓨터공학부

홍 기 훈

Abstract

Autostereoscopic Three-dimensional Imaging Methods using Holographic Recording Techniques on Photopolymer

Keehoon Hong

Department of Electrical and Computer Engineering

Seoul National University

The novel holographic recording techniques suggested in this dissertation are experimentally investigated to improve the limitations of conventional autostereoscopic three-dimensional (3D) displays. Two types of holographic recording techniques for implementing novel autostereoscopic 3D imaging methods are presented in this dissertation work: i) hogel overlapping method for enhancing lateral resolution of a holographic stereogram, and ii) lens-array holographic optical element (HOE) for providing a see-through property in an integral imaging method.

Photopolymer film is used as a holographic material in this work. Dosage responses of a single wavelength and a three-wavelength multiplexed hologram recorded in the photopolymer film are presented. See-through property and diffraction efficiencies of the three-wavelength multiplexed hologram recorded in the photopolymer film are evaluated by the display experiments. Additionally, shrinkage of the photopolymer film is theoretically analyzed and measured by the experiments.

The hogel overlapping method for a holographic printing technique is proposed to enhance the lateral resolution of holographic stereograms. A numerical analysis by computer simulation shows that there is a limitation on decreasing the hogel size while recording holographic stereograms. Instead of reducing the size of hogel, the lateral resolution of holographic stereograms can be improved by printing overlapped hogels. An experimental setup for holographic printing is built, and two holographic stereograms using the conventional and proposed overlapping methods are recorded, respectively. The resultant images from the experimentally generated holographic stereograms make a comparison between the conventional and proposed methods. The experimental results confirm that the proposed hogel overlapping method improves the lateral resolution of holographic stereograms compared to the conventional holographic printing method.

The lens-array HOE is suggested for a see-through 3D imaging based on the integral imaging. The full-color lens-array HOE provides a see-through property with three-dimensional virtual images. An HOE recording setup is built, and the full-color lens-array HOEs are recorded by using holographic recording techniques of a spatial and wavelength multiplexing. The experimental results confirm that the suggested method can provide the full-color 3D virtual images with the see-through property. The viewing characteristics of the presented autostereoscopic 3D display are evaluated by the optical parameters of the lens-array HOE. Two lens-array HOEs with different optical parameters are fabricated to have both functions of the two-dimensional (2D) and 3D transparent screens. Display experiments for the 2D and 3D imaging on the proposed transparent screens are carried out, and the viewing characteristics in both cases are discussed. The autostereoscopic 3D display using the lens-array HOE can provide dynamic 3D virtual images because it has an external spatial light modulator. The dynamic elemental images are generated by computer graphics, and the feasibility of displaying

the dynamic 3D virtual images on the lens-array HOE is experimentally verified.

Keywords: Autostereoscopic three-dimensional display, holographic printing, holographic optical element, volume hologram, integral imaging, photopolymer.

Student Number: 2008-21006

Contents

List of Tables

List of Figures

Chapter 1 Introduction

1.1 Background and current issues of autostereoscopic three-dimensional display

Three-dimensional (3D) display technologies are divided into two categories: stereoscopic and autostereoscopic 3D display [1-6]. The stereoscopic 3D display provides a depth perception for the viewer by means of stereopsis for a binocular disparity [7, 8]. The basic principle of the stereoscopic 3D display is to present two different offset images that are provided separately to the viewer's right and left eyes. The binocular vision of a human visual system merges the two offset images into a single image which has a feeling of the 3D perception [9, 10]. The stereoscopic 3D displays require viewers to wear special glasses in order to see the appropriate offset images in the two different eyes. Generally, the stereoscopic 3D displays are categorized according to the types of the glasses: anaglyph, polarization, and liquid crystal (LC) shutter glasses [2, 3]. In recent years, stereoscopic 3D display has been successfully commercialized for 3D movies, sports broadcasting,

and television markets [11-14]. However, the stereoscopic 3D displays still suffer from various problems, such as a visual fatigue from the accommodation-convergence mismatch [15-18] and feeling of discomfort due to the use of the special glasses.

To develop more realistic 3D display, which does not require any glasses and is free from the visual fatigues, the trend of 3D display research has changed from the stereoscopic 3D display to the autostereoscopic 3D display [19, 20]. The autostereoscopic 3D display is often called a glasses-free or glassless 3D display because it does not require any special headgear or glasses which are essential in the stereoscopic 3D display. From a viewpoint of the glasses-free 3D display, multi-view display, integral imaging, and even holography can be included in the scope of the autostereoscopic 3D display. The multi-view display and integral imaging method in the autostereoscopic 3D display category are based on flat panel display (FPD) technologies. Both methods use additional optical layers in front of the FPD to create autostereoscopic 3D images. The holography, invented by Dennis Gabor in 1948, is a 3D display technique that allows the wavefronts of light scattered from an object to be recorded and later reconstructed so that the viewers can see 3D images of the recorded object even when it is no longer present in the scene. The hologram, which is a

recording of object's light on the holographic material by holography technique, stores all the characteristics of light from the object including phase, amplitude, and wavelength. Although the holography is thought to be an ideal technology for the 3D display, it has tremendous technical challenges to implement practical 3D display systems by nowadays technologies.

In recent years, development in digital devices has led to widespread use of FPDs, especially an LC display, and it has facilitated efforts on the academia and industry to commercialize the autostereoscopic 3D display based on the FPD. Generally, the autostereoscopic 3D display based on FPDs has double layered structure consisted of the FPD and an optical layer as shown in Fig. 1.1. A spatial light modulator (SLM) in the FPD modulates intensities of light from a light source to generate a two-dimensional (2D) image. The optical layer attached in front of the FPD generates a number of perspective images by distributing light rays from the 2D image, which is generated by the FPD, to multiple view-points in a viewer's direction. The viewers in different view-points can observe different perspective images, and therefore the depth perception by the binocular disparity, convergence, and motion parallax can be realized. Examples of the optical layers are one-dimensional (1D) periodic optical structures such as a parallax barrier and

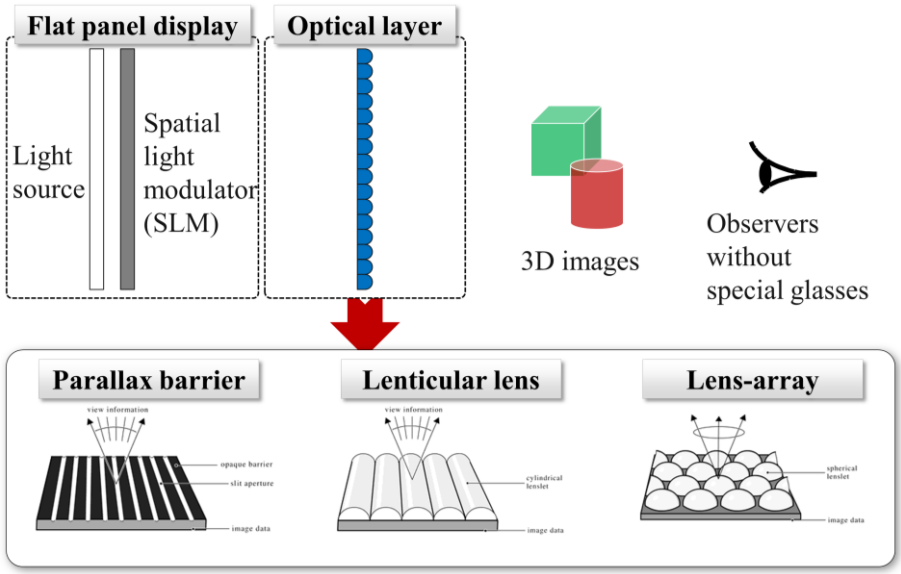

Figure 1.1 A schematic diagram of the autostereoscopic 3D display and examples of conventional optical layers.

lenticular lens for the horizontal parallax only multi-view display, and 2D periodic optical structure of a lens-array for the full parallax integral imaging method.

Even though the FPD-based autostereoscopic 3D display has received attention to become a next generation commercial 3D display following the stereoscopic 3D display, there still remains several issues to be solved. The issues on the FPD-based autostereoscopic 3D display can be discussed separately on its composing components which are the FPD and optical layer.

First issue on the FPD is a spatial resolution of the SLM. When 3D images are displayed through the optical layer, the spatial resolution of the SLM is sacrificed to gain directional information for generating the perspective images. For example, the multi-view display which provides N view-points has $1/N$ of native resolution of the SLM. In other words, the resolution of 3D images displayed by the FPD-based autostereoscopic 3D display is proportional to that of SLM in the FPD. Though higher resolution or smaller pixel size of the SLM is favorable to display high quality 3D images, the size of pixel cannot be reduced infinitesimally.

Another issue on the FPD for autostereoscopic 3D display is a difficulty to apply it to other applications such as an augmented reality or optical 3D screen. Since the FPD itself is not a transparent device, sight of the viewer is

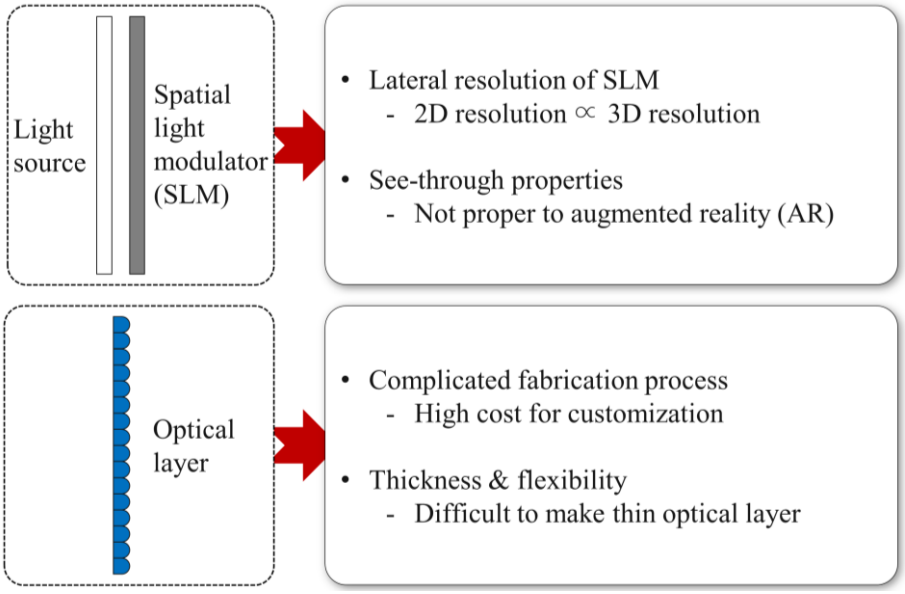

Figure 1.2 Issues on the autostereoscopic 3D display using the conventional optical layers and flat panel display.

blocked by the FPD and the real-world scene behind the device cannot be provided to them. A see-through property is necessary on the both FPD and optical layer to apply the FPD-based autostereoscopic 3D display into those applications.

Some issues also rise about the optical layer structure. The parallax barrier for the optical layer has advantages on an easy fabrication and suitability for a 2D/3D convertible feature. However, it has severe drawbacks of the reduced brightness because fraction of light from the FPD is blocked by the parallax barrier itself. On the other hand, optical layers which have a periodic lens structure, such as the lenticular lens and lens-array, have much higher optical efficiency compared to the parallax barrier. Another issue on those optical layers is a difficult fabrication process, such as a compression or etching methods. It also has difficulties on customizing its optical properties due to those of complicated fabrication processes. Moreover, a certain thickness is required in order to perform a lens function, thus it is hard to make the optical layer in a thin structure. Issues on the FPD-based autostereoscopic 3D display are summarized on Fig. 1.2.

1.2 Motivation of this dissertation work

A holographic recording technique can be a breakthrough to overcome the limitations on the current autostereoscopic 3D display discussed in the previous section. Although the holography itself is one category of the autostereoscopic 3D display, the holographic recording techniques on holographic materials have been widely applied to implement 3D displays by virtue of its beneficial characteristics for display applications.

The advantages of adopting the holographic recording techniques to the autostereoscopic 3D display are summarized in Fig. 1.3. The resolution limit of the holographic material is much smaller than that of the conventional SLM. For example of the holographic materials, a silver halide which has grain size of 8 nm was recently reported [21]. With these holographic materials, a huge amount of image information, which means a high resolution image, can be stored in the holographic material by proper optical arrangements in the holographic recording setup. A holographic optical element (HOE) is another way to apply the holographic recording techniques to the 3D display [22, 23]. When the HOE is adopted in the 3D display system, an image projector replaces SLM for providing intensity modulated images. In this case, lateral resolution of provided images on the HOE is

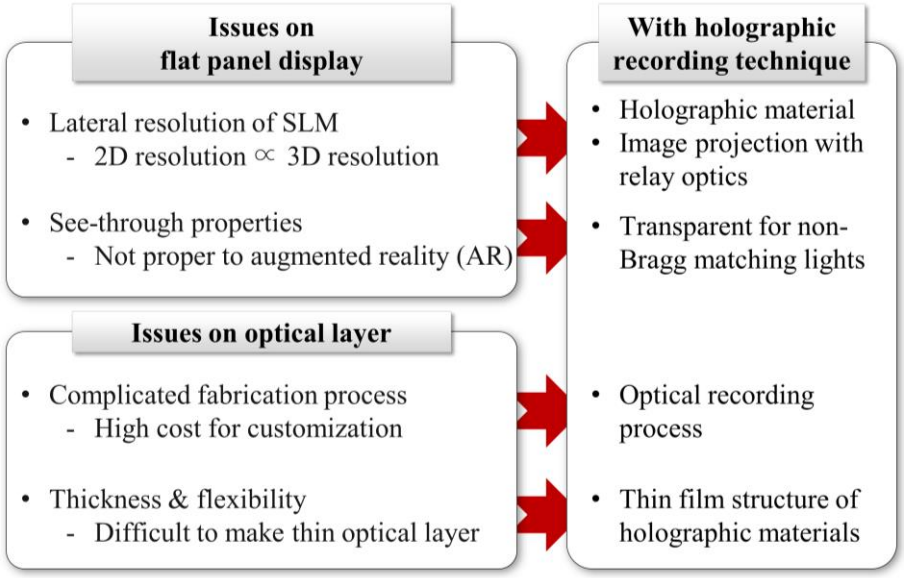

Figure 1.3 Advantages of the autostereoscopic 3D display which adopts the holographic recording techniques.

proportional to those of the image projector, and it can be enlarged by using demagnifying relay optics for the image projector.

Angle and wavelength selective characteristics of a volume hologram by Bragg's law can be also an advantage for applying the holographic recording techniques to the autostereoscopic 3D display. Since the volume hologram only diffracts light which satisfies Bragg condition, it has the see-through characteristic and behaves like a transparent film for Bragg unmatched light. Therefore, the autostereoscopic 3D display with the see-through characteristic realized by the holographic recording technique is perfectly suitable for the optical see-through 3D augmented reality (AR) applications.

If the optical layer in the conventional autostereoscopic 3D display can be implemented by the holographic recording techniques, the problems of complicated fabrication process and thickness for the conventional optical layers can be improved. Holographic recording can be simply performed by an optical recording process, and it has advantages on a mass production with low cost. Furthermore, since most of holographic materials have a thin film structure, the optical layer implemented on the holographic material by the holographic recording techniques can have a narrow thickness.

1.3 Objective and scope of this dissertation

The objective of this dissertation is to overcome the limitations of the conventional FPD-based autostereoscopic 3D display by adopting the holographic recording techniques to replace their composing components with holograms recorded on the holographic material. For this purpose, two holographic recording techniques are developed in this dissertation. One is a holographic printing technique which can replace the SLM and optical layer in the conventional autostereoscopic 3D display with a holographic stereogram. Another one is a hologram recording technique for fabricating HOEs which can replace the optical layer of the conventional autostereoscopic 3D display.

Before describing these holographic recording techniques, the optical characteristics of the photopolymer, which is a holographic material used for the experiments in this dissertation, are analyzed in Chapter 2. In Chapter 2, principles of refractive index modulation in the photopolymer is introduced. Then, the optical characteristics of the dosage responses, wavelength multiplexing, and shrinkage for the photopolymer are experimentally evaluated.

Chapter 3 describes a proposed holographic printing technique with a

novel hogel overlapping method for enhancing the lateral resolution of holographic stereograms. Principles of the holographic printing are described, and the limitation on enhancing lateral resolution of the holographic printing is numerically analyzed. The proposed hogel overlapping method is verified by comparing two holographic stereograms which are recorded by conventional and proposed methods.

In Chapter 4, a full-color lens-array HOE which can replace the optical layer of the integral imaging is presented. Holographic recording technique for fabricating the full-color lens-array is described. The feasibility of displaying autostereoscopic 3D images on the proposed structure with the see-through property is verified by the experiments. Furthermore, viewing characteristics of the lens-array HOE are evaluated, and possibility to use the lens-array as 2D/3D transparent screens is described. Finally concluding remarks of this dissertation are made in Chapter 5. The objective and scope of this dissertation are graphically depicted in Fig. 1.4.

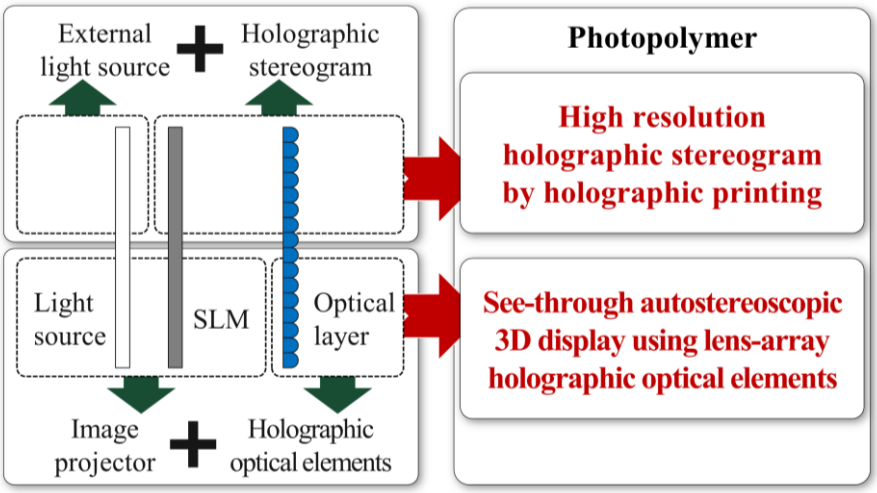

Figure 1.4 Objective and scope of this dissertation.

Chapter 2 Photopolymer film for holographic material

2.1 Introduction

Holographic material, which is photosensitive, can store the interference pattern between signal and reference waves by modulating their transmittance or refractive indexes during the holographic recording procedure. The holographic material is usually used for implementing holographic imaging or holographic optical elements [24-27]. The optical performances of the recorded hologram strongly depend on the characteristics of the holographic material. Therefore, selection of a suitable holographic material is important for the optical quality of the generated hologram. Important material parameters for the holographic material are diffraction efficiency, photosensitivity, dimensional stability, manufacturing process, dynamic range, and so on [26]. The light efficiency of the hologram is determined by the diffraction efficiency of the holographic material, which

is related to the refractive index contrast and thickness of the material. The recording speed and the amount of required exposure energy for generating the hologram are determined by the photosensitivity of the holographic material. Properties of holographic material, such as dimensional stability, linearity, and volatility, affect the fidelity of the recording and reconstruction procedure. The holographic materials with a high dynamic range makes it possible to do wavelength and spatial multiplexing for color imaging and large-sized recording, respectively. For commercial usage of holograms, simplicity of the manufacturing process is necessary for low-cost and high-quality manufacturability.

There are several candidates for the holographic material such as silver halide, photorefractive polymer, photoresist, dichromated gelatin, photo-thermoplastics, photopolymer, and so on [24, 27-31]. Each of them has different material characteristics, which are listed in Table. 2.1. The silver halide is the most widely used holographic material due to their high sensitivity to various wavelengths. However, it requires wet processes such as developing and bleaching to complete the hologram recording. The photorefractive polymer has the advantage of its rewritable property. Paradoxically, it has a problem in reconstructing the original waves without erasing the hologram. Photoresist is a photosensitive material that can be

used to make surface relief holograms. It has the advantage of mass replication by transferring its surface relief to other soft materials. However, the photoresist has a limited maximum diffraction efficiency and quite low photosensitivity. Dichromated gelatin is an attractive holographic material for the volume hologram recording because it has low scattering and absorption, high diffraction efficiency and spatial resolution. However, it requires careful control conditions for the hologram recording and has relatively low sensitivity and limited range of wavelengths. Photo-thermoplastic is a reusable holographic material which changes its surface to modulate the refractive index by the exposed light intensity by help of electric forces. It suffers from ghost images after recording and decrease in diffraction efficiency with repeated write-erase recycling. The advantages of the photopolymer are easy treatment after exposure and relatively high sensitivity and diffraction efficiency [32-36]. Photo-curing is only needed to bleach the absorbing species fully to gain optimal transparency. A drawback of the photopolymer is its shrinkage characteristics during the hologram recording procedure. The shrinkage on the photopolymer affects the diffraction angle of the reconstructed signal beam and the diffraction efficiency. Among these candidates for the holographic material, the photopolymer has been used for the experiments in this dissertation work.

Table 2.1 Characteristics of holographic materials.

	Hologram type	Processing	Rewritable	Maximum efficiency [%]	Required exposure [mJ/cm^2]	Resolution limit [mm^{-1}]
Silver halide	Amplitude and phase	Wet	No	> 70	0.001 – 0.1	1,000 – 10,000
Photorefractive polymer	Phase	High voltage (~kV)	Yes	~ 100	1 – 1,000	2,000 – 5,000
Photoresist	Phase	Wet	No	~ 30	~100,000	10,000
Dichromated gelatin	Phase	Wet	No	~ 90	2 – 250	10,000
Photo-thermoplastic	Phase	Voltage	Yes	> 40	~1000	2,000
Photopolymer	Phase	Post exposure	No	~ 100	0.1 – 50,000	2,000 – 10,000

2.2 Principles of refractive index modulation in photopolymer film

Generally, the photopolymer stores phase information contained in the light by changing the refractive index of the composing materials in proportion to the intensity of the holographic interference patterns [26, 28]. Since the hologram recorded on the photopolymer is a volume hologram, it has the advantage of high angular selectivity by Bragg's law for the incident reference light [25]. Furthermore, multiple holograms can be superimposed in the same volume area of the photopolymer, which is called multiplexed hologram, when the photopolymer has enough thickness and material index change for a high dynamic range. This multiplexing technique on the photopolymer gives it the additional advantages of full-color recording and ability to record large-sized hologram by the wavelength and spatial multiplexing, respectively [37-40].

Figure 2.1 shows a typical model of hologram formation in the photopolymer [26, 41-32]. Generally, the photopolymer is composed of a total of three main components: photo-initiator, monomers, and host matrix components. The host matrix provides mechanical stability and ensures optical properties such as transparency and surface flatness. During

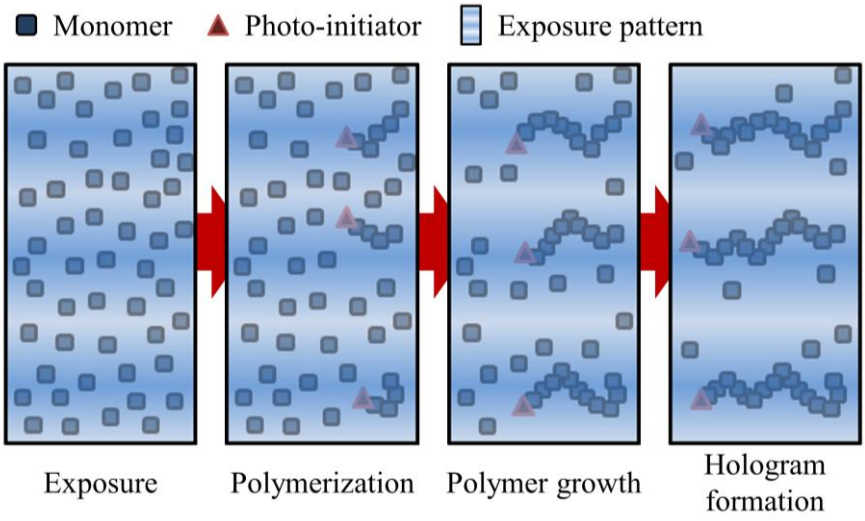

Figure 2.1 A schematic diagram of a polymerization process in the photopolymer for the refractive index modulation.

the holographic recording, the light intensity of the optical interference pattern on the photopolymer activates the photo-initiator and the monomers begin to grow into polymers [32-46]. Polymerization is induced in the constructive interference area of the photopolymer, while little or no polymerization occurs in the destructive interference area. The patterned polymerization forms a concentration gradient in the unreacted monomers. Thus, the unpolymerized monomers diffuse from the destructive to constructive interference area to equalize its concentration in the material. This polymerization process ends when there are no more monomers to be polymerized or the left monomers cannot diffuse into the active area. The difference of the refractive index between the polymerized area and the host material leads to the modulation of refractive index.

The holograms recorded in the photopolymer by these procedures are phase hologram because the refractive index pattern inside the photopolymer is modulated by the holographic interference pattern which has phase information in the signal and reference waves.

The photopolymer used for the hologram recording experiments in this dissertation has a layered film structure as illustrated in Fig. 2.2(a). This photopolymer is provided from Bayer MaterialScience. A photopolymer layer has a thickness of 14 um – 18 um, and it is coated on a flexible plastic

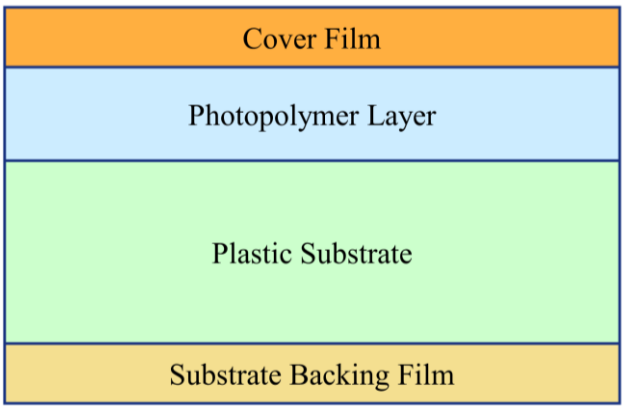

(a)

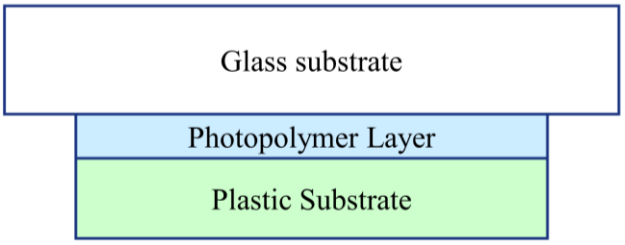

(b)

Figure 2.2 Photopolymer film: schematic diagrams of its layered structure (a) before and (b) after the pre-handling for the hologram recording.

substrate which has a thickness of 175 um. The photopolymer layer has a self-adhesive property. Since the plastic substrate is optically clear, it does not decrease the amount of dosage energy. The photopolymer on the plastic substrate is sandwiched between the cover and substrate backing films. These two layers prohibit the photopolymer layer from air contact before the hologram recording in addition to the purpose of protection. Pre-handling is needed on this layered structure for the hologram recording. The two protection layers are removed and the remaining layers are laminated on a glass substrate by the self-adhesive property of the photopolymer layer as shown in Fig. 2.2(b).

2.3 Dosage response of photopolymer film for the hologram recording in a reflection geometry

A change in the refractive index of the photopolymer is related to the dosage energy of the exposed laser during the hologram recording procedure. The dosage response is determined dominantly by the characteristic of the photo-initiator in the photopolymer. There are several types of photo-initiator which have different photo-sensitivities to different ranges of wavelength. The photopolymer film used in the hologram recording has more than three different photo-initiators to enable it to form polymerization for the wavelengths covering the visible range.

The photopolymer film is suitable for full-color hologram recording due to its photo-sensitivity covering the wavelengths of the visible range. The full-color hologram can be generated by multiplexing three different holograms recorded at the wavelengths of three primary colors of red, green, and blue. The polymerizations initiated by the photo-initiators at the three wavelengths generate independent grating patterns with different changes of refractive index. As a result, the changes of refractive index at different wavelengths are measured as diffraction efficiencies in the reconstruction procedure. The diffraction efficiency is proportional to the change of the

refractive index. During the full-color hologram recording by wavelength multiplexing technique, similar diffraction efficiencies should be achieved at the three primary wavelengths to represent appropriate colors in the reconstruction procedure. To achieve those diffraction efficiencies in the full-color hologram, the examination of dosage responses is required for single wavelength recordings at the three primary wavelengths.

Hologram can be generated on the photopolymer film by either transmission or reflection geometry in the recording procedure. In the transmission hologram, the object and reference beams are incident on the holographic material from the same side. On the other hand, the object and reference beams are incident on the holographic material from opposite surfaces in the reflection hologram. It is well known that the transmission and reflection holograms have high selectivity from angle and wavelength, respectively. Therefore, angle multiplexed holograms are typically recorded by the transmission scheme, and wavelength multiplexed holograms employ the reflection scheme for the hologram recording.

All holograms implemented in this dissertation are recorded by using a reflection scheme for generating the full-color hologram by wavelength multiplexing as shown in Fig. 2.3(a). In the recording procedure, the reference and signal beams are incident on the pre-handled photopolymer

layer in the opposite directions with the incident angle of α and β, respectively. The incident power densities of the reference and signal beams are designated as P_R and P_S, respectively. In the reconstruction procedure, as shown in Fig. 2.3(b), the signal beam is blocked and only the reference beam is projected to the recorded photopolymer film with the same incident angle α which is used in the recording procedure. The signal beam is then reproduced by the diffraction from a recorded grating in the photopolymer film. However, the incident reference beam in the reconstruction procedure cannot be fully diffracted by the grating, and a portion of it transmits through the photopolymer film. When the power densities of the transmitted and diffracted beams are P_T and P_D, respectively, the diffraction efficiency, η, of the hologram recorded in the photopolymer film can be obtained by

$$\eta = \frac{P_D}{P_D + P_T}. \tag{2.1}$$

The dosage response to the diffraction efficiency of the photopolymer film is examined using two plane waves recording in the three different wavelengths of 473 nm, 532 nm, and 671 nm, which correspond to the primary colors of blue, green, and red, respectively. The relationship between the diffraction efficiency and dosage energy at a single wavelength is first evaluated. The reflection geometry is used for the hologram recording

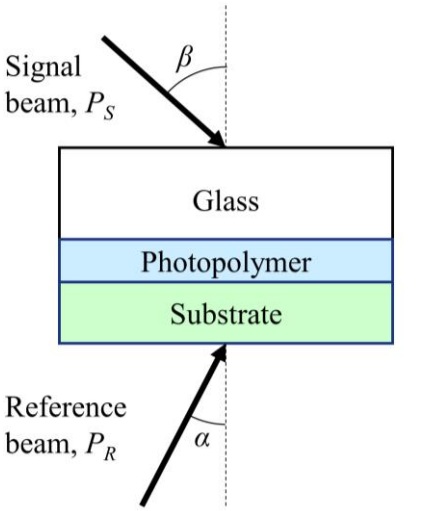

(a)

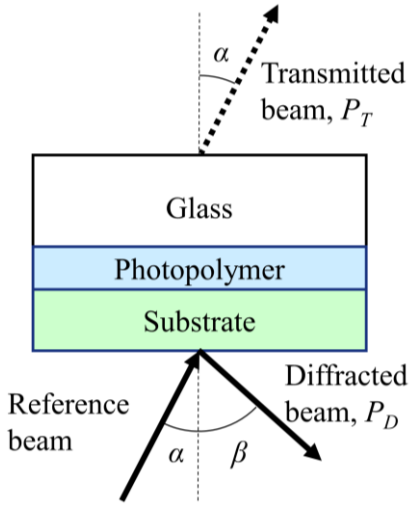

(b)

Figure 2.3 Schematic diagrams of (a) recording and (b) reconstruction of the reflection hologram on the photopolymer film.

scheme with incident angles of 0° and 45° for the signal and reference plane waves, respectively. Three diode pumped solid state (DPSS) lasers which have wavelengths of 473 nm, 532 nm, and 671 nm, are used for the light sources. Figure 2.4 shows the diffraction efficiency versus the total dosage response for two-beam plane wave reflection gratings at the three wavelengths. The total dosage energy is controlled by changing the exposure time while the power densities of the signal and reference wave are fixed. The power densities of the signal and reference waves are set to be 0.71 mW/cm^2 and 0.89 mW/cm^2 for 671 nm wavelength, 4.5 mW/cm^2 and 5.3 mW/cm^2 for 532 nm wavelength, 3 mW/cm^2 and 3.8 mW/cm^2 for 473 nm wavelength, respectively.

As shown in Fig. 2.4, gratings are not generated in the low energy dosage region which is an inhibition dosage region. Inhibition dosages are different in accordance with the wavelength used in the hologram recording. After the inhibition dosage region, gratings begin to form at the dosage energy of 2 mJ/cm^2, 8 mJ/cm^2, and 3.5 mJ/cm^2 for 671 nm, 532 nm, and 473 nm wavelengths, respectively. Gratings are grown with a non-linear property and start to saturate around the dosage energy of 30 mJ/cm^2 for the three wavelengths. Power densities of the transmitted and diffracted waves are measured by an optical power meter at the saturated condition, and

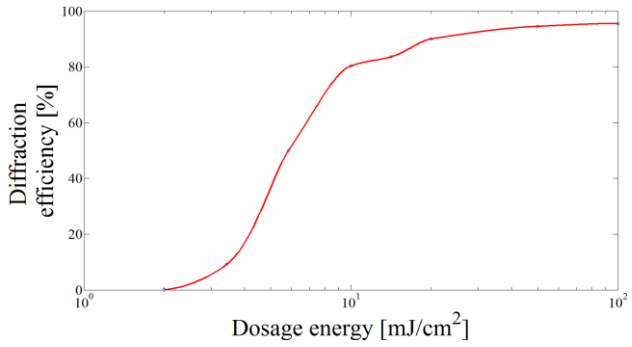

(a)

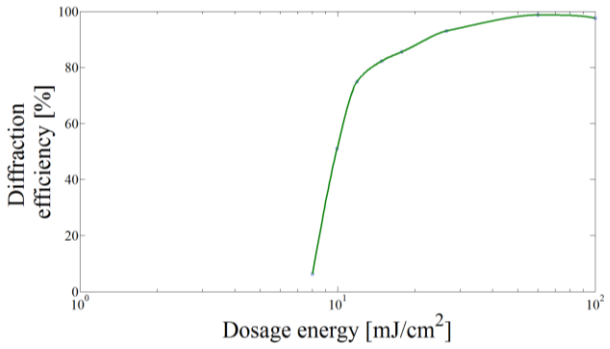

(b)

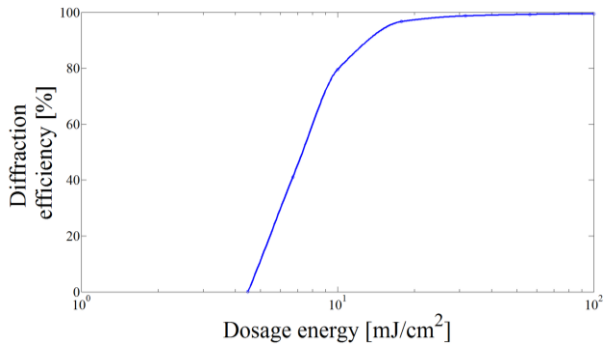

(c)

Figure 2.4 Dosage curves for the single wavelength recordings using (a) red (671 nm), (b) green (532 nm), and (c) blue (473 nm) lasers.

diffraction efficiencies are obtained by Eq. (2.1). The saturated diffraction efficiencies for 671 nm, 532 nm, and 473 nm wavelengths are 95.5 %, 97.6 %, and 99.5 %, respectively.

A human eye has three kinds of cone cells which sense three different wavelength ranges corresponding to the primary colors of red, green, and blue, in the visible spectrum [47, 48]. Typically, most of display technologies use these primary colors to represent the full-color imaging which can be perceived by a human visual system [49, 50]. For the purpose of the full-color imaging on the hologram, three lasers which have wavelengths of 671 nm (red), 532 nm (green), and 473 nm (blue) are used in the hologram recording procedure by the wavelength multiplexing technique. To display proper colors on the wavelength multiplexed hologram, it is necessary to design appropriate diffraction efficiencies for red, green, and blue wavelengths. This color management during the recording and reconstructing holograms can be described by the colorimetry analysis [47, 48]. With the colorimetry analysis, representable colors by selected wavelengths of the primary colors can be defined in a color space. For the lasers used in this dissertation, a theoretical color gamut is shown in Fig. 2.5. To express this color gamut in the wavelength multiplexed hologram, however, the hologram necessarily needs to diffract lights at each primary wavelength in the

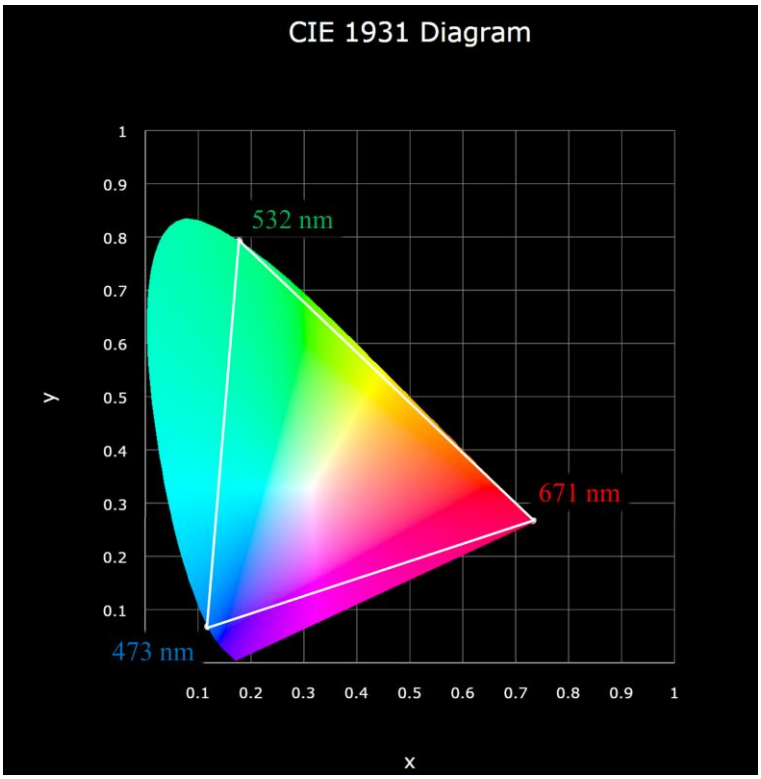

Figure 2.5 Theoretical color gamut for the three-wavelength multiplexed hologram using lasers which have wavelengths of 671 nm, 532 nm, and 473 nm.

reconstruction procedure. Therefore, similar diffraction efficiencies at the primary wavelengths are the most important consideration in the wavelength multiplexing technique. Exposure conditions during the hologram recording with the wavelength multiplexing are directly related to the diffraction efficiencies at the primary wavelengths.

To get an appropriate exposure condition, the wavelength multiplexing is examined by the two-plane wave recording using laser light sources of three different wavelengths of 473 nm, 532 nm, and 671 nm. Generally, there are two approaches to the wavelength multiplexing. One is a hologram recording with a sequential exposure, and another is a recording using simultaneous exposure of three different wavelength lasers.

Since the latter approach has the advantages of short recording time and easiness of getting exposure condition, the simultaneous exposure method is preferable for the wavelength multiplexing. In order to optimize the exposure condition to get similar magnitudes of diffraction efficiencies for the three wavelengths, the three lasers are exposed simultaneously on the photopolymer, while varying the power densities of the lasers individually. Table 2.2 shows the exposure conditions to obtain the similar diffraction efficiencies at the three wavelengths in the full-color recorded hologram.

The transmittance of the full-color recorded hologram generated by the

exposure condition listed in Table 2.2 is measured by the optical spectrometer, and it is shown in Fig. 2.6. The diffraction efficiency of the recorded hologram in the photopolymer can be considered as a portion of light excluding the transmitted light, which is expressed as 1-*T*, when the reflectance and absorption in the photopolymer film are negligible. The measured values of the transmittances for 671 nm, 532 nm, and 473 nm are 41.1 %, 40.8 %, and 40.3 %, respectively. Therefore, the recorded full-color hologram results in the complementary values of diffraction efficiencies of 48.9 %, 49.2 %, and 49.7 % at 671 nm, 532 nm, and 473 nm wavelengths, respectively. These results show that the photopolymer film used in the hologram recording is well-suited for the use of the full-color hologram recording.

The display experiments are performed to verify the feasibility of the full-color hologram recorded on the photopolymer film as an imaging device. Incoherent imaging devices are used in the display experimental setup because most of display devices do not use lasers for their light source. Figure 2.7 shows a display experimental setup for the full-color hologram. Since the full-color hologram is recorded using a collimated reference beam in the hologram recording procedure, the images projected on the full-color hologram should be also a collimated light for satisfying the Bragg condition.

Table 2.2 Exposure conditions to record three color wavelength multiplexing on the photopolymer film.

Power density [mW/cm^2]						Exposure Time [s]
Red (671 nm)		Green (532 nm)		Blue (473 nm)		
Signal	Reference	Signal	Reference	Signal	Reference	20
0.3063	0.4422	1.058	0.9223	0.951	0.724	

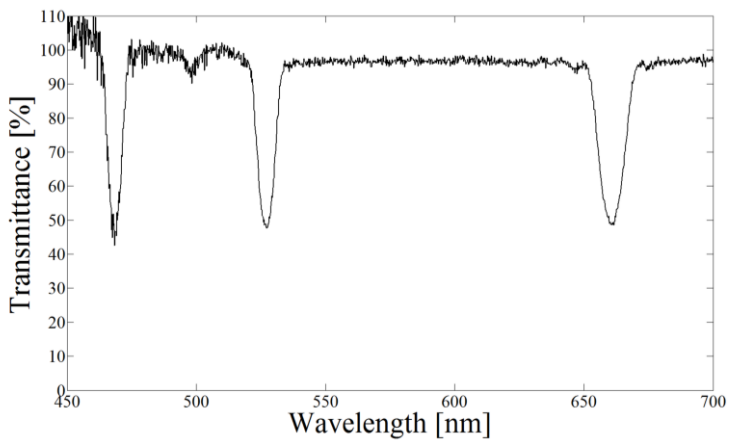

Figure 2.6 Measured transmittance of the full-color recorded hologram using the exposure condition listed in Table. 2.2.

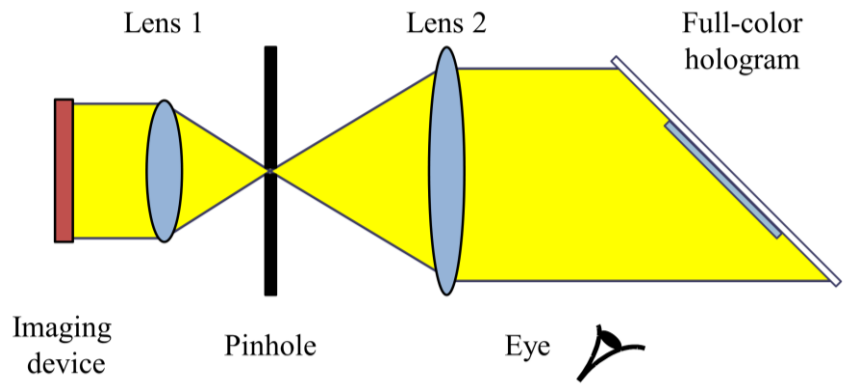

(a)

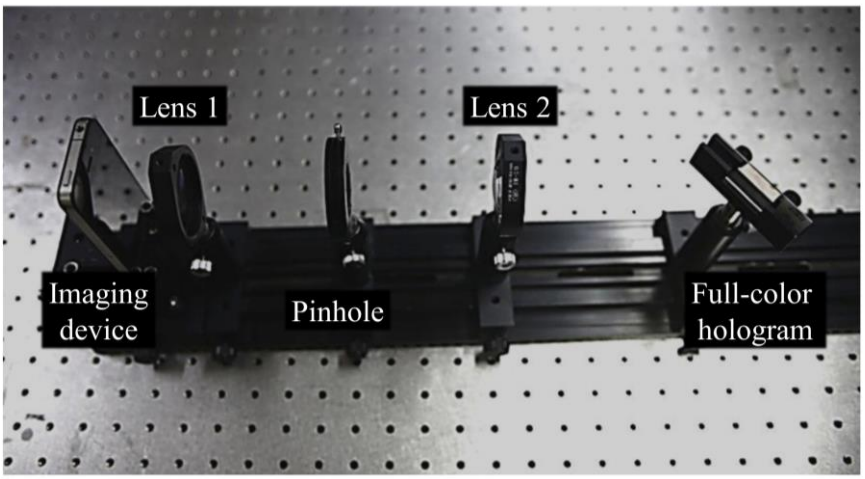

(b)

Figure 2.7 Experimental setup for displaying images on the full-color hologram using incoherent imaging device: (a) schematic diagram and (b) captured image of the display experimental setup.

For this reason, the display experimental setup has collimating optics consisting of two lenses and a pinhole. The pinhole is located on the focal plane of the two lenses, and both lenses function as a 4-f system. When the pinhole is small enough, diffused light from the imaging device is filtered by the pinhole and only a collimated light can pass through the collimating optics. To verify the full-color imaging on the full-color hologram, the image of a sub-pixel structure in the LCD, shown in Fig. 2.8(a), are displayed on the imaging device in the display experimental setup. Figure 2.8(b) shows the resultant diffracted images from the full-color hologram in the display experiments. It is clearly demonstrated in the experiments that the three primary colors are successfully displayed with nearly the same diffraction efficiencies.

Additionally, a see-through property of the hologram recorded in the photopolymer is observed in the resultant images. Since the hologram recorded in the photopolymer is a volume hologram, it diffracts only Bragg matched lights from the imaging device, and Bragg mismatched light from the background scene passes through without feeling it as the hologram.

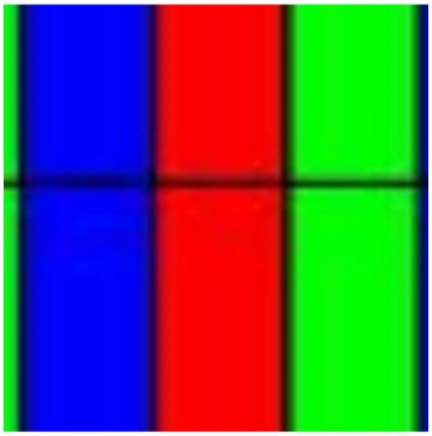

(a)

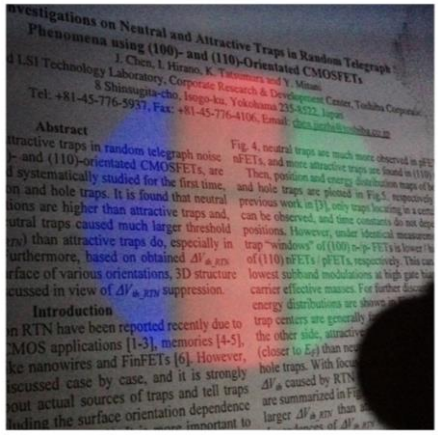

(b)

Figure 2.8 (a) Images displayed on the imaging device and (b) diffracted images from the full-color hologram by the display experimental setup shown in Fig. 2.7.

2.4 Shrinkage characteristic of photopolymer film

The major disadvantage of the photopolymer is a grating detuning effect which is due to the dimensional change, or shrinkage, of the photopolymer by a chemical reaction during the hologram recording and curing procedures [51-54]. The dimensional change in the hologram recorded photopolymer results in formation of a grating which has different grating spacing compared to that of the interference fringes between the signal and reference waves. Consequently, Bragg condition is mismatched and the recorded volume hologram cannot be completely reconstructed. Therefore, it is important to know how the grating detuning by the shrinkage influences the readout of the hologram.

In this section, we examine shrinkages on the photopolymer film along the thickness and length directions by analyzing optically measured diffraction angle and Bragg curves, instead of measuring the changes in physical thickness and length of the photopolymer directly.

Figure 2.9(a) shows a schematic diagram of recording geometry for the reflection hologram [51]. In the figure, the photopolymer, which has a refractive index of n, has the thickness and length of d and l, respectively, before the dimensional change. θ_{1a} and θ_{2a} are incidence angles of the object

and reference beams, respectively. The fractions of dimensional changes are assumed to be α_l and α_d along the length and thickness directions, respectively. Each of the periods for the recorded gratings before and after shrinkage is denoted by Λ and Λ', respectively.

According to Snell's law, the reference and object beams are refracted in the photopolymer and change the incidence angles to $\theta_1=\cos^{-1}[\cos(\theta_{1a})/n]$ and $\theta_2=\cos^{-1}[\cos(\theta_{2a})/n]$. The refractive index of the material is also changed to $(1+\alpha_n)n$. The grating vector recorded by the signal and reference waves can be written as,

$$\bar{K} = \frac{2\pi}{\Lambda}\left(\sin\theta_0 x + \cos\theta_0 z\right), \tag{2.2}$$

where $\theta_0=(\theta_1 - \theta_2)/2$ and grating spacing Λ is

$$\Lambda = \frac{\lambda}{2n\sin\left(\frac{\theta_1+\theta_2}{2}\right)}. \tag{2.3}$$

After the dimensional change, the grating vector will be changed to

$$\bar{K}' = \frac{2\pi}{\Lambda}\left(\frac{1}{1+\alpha_l}\sin\theta_0 x + \frac{1}{1+\alpha_d}\cos\theta_0 z\right). \tag{2.4}$$

When a readout beam is incident at the incidence angle identical to that of the reference beam in the recording procedure, a phase mismatch ΔK will

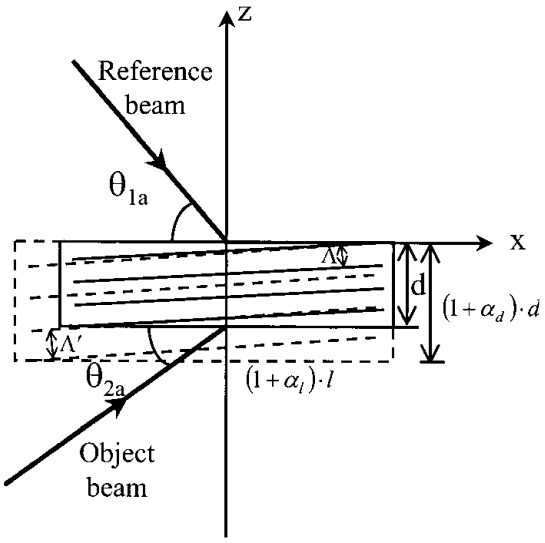

(a)

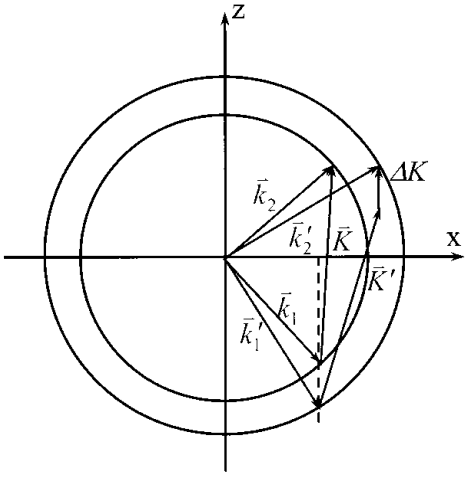

(b)

Figure 2.9 (a) A schematic diagram of dimensional changes in the photopolymer by the shrinkage, and (b) a K-vector diagram for the recorded reflection hologram [51].

occur along the *z*-axis and can be written as

$$\Delta K = k_{1z}^{'} + K_{z}^{'} - k_{dz}, \tag{2.5}$$

where $K_{z}^{'}$ and $k_{1z}^{'}$ are the wave vectors of the detuned grating and readout beams along the *z*-axis, respectively. k_{dz} is the wave vector of the reconstructed beam along the *z*-axis, and can be represented by

$$k_{dz} = \left\{ [(1+\alpha_n)n]^2 - \left[\cos\theta_{1a} + \frac{1}{1+\alpha_l}(\cos\theta_{2a} - \cos\theta_{1a}) \right]^2 \right\}^{1/2}. \tag{2.6}$$

As a result, the angular shift of the reconstructed beam is given by

$$\Delta\theta_d = \theta_{2a}^{'} - \theta_{2a} = \cos^{-1}\left[\cos\theta_{1a} + \frac{1}{1+\alpha_l}(\cos\theta_{2a} - \cos\theta_{1a}) \right] - \theta_{2a}, \tag{2.7}$$

where $\theta_{2a}^{'}$ is the direction of the reconstructed wave diffracted from the dimensionally changed volume grating after the shrinkage. Equation (2.7) indicates that the reconstruction angle depends only on shrinkage (α_l) and the recording angles. If the photopolymer has no shrinkage along the length direction, the direction of reconstructed wave is maintained identically to that of the signal beam used in the recording procedure.

The shrinkage characteristics, α_l and α_d, of the photopolymer film used in the hologram recording experiments for this dissertation are measured by

the experiments. For recording the volume grating on the photopolymer film, a green laser (λ=532 nm) is used, and the incidence angles of the reference (θ_{1a}) and signal (θ_{2a}) beams are 90˚ and 40˚, respectively. Figure 2.10(a) shows an experimental setup for measuring α_l. In this setup, the direction of reconstructed beam is measured by an optical power-meter with a motorized linear stage, and the measured direction is compared with the direction of the signal beam to obtain the angular shift between the reconstructed and signal beams as discussed in Eq. (2.7). In the figure, the reconstruction and signal beam paths are indicated by blue and red lines, respectively. As shown in Fig 2.10(b), the peak intensities are measured at the same location for both the reconstructed and signal beams, which means that both beams have the same beam path, and thus there is no angular shift between them. From Eq. (2.7), the angular shift ($\Delta\theta_d$) vanishes only when the photopolymer has no shrinkage along the length direction (α_l=0). Therefore, the experimental results confirm that the photopolymer used in the experiments has no shrinkage along the length direction (α_l=0).

To find out the shrinkage on the thickness direction, Bragg curve of the volume hologram recorded on the photopolymer is measured by the experimental setup shown in Fig. 2.11(a). The measured Bragg curve is compared to the computer simulated Bragg curves calculated by the coupled

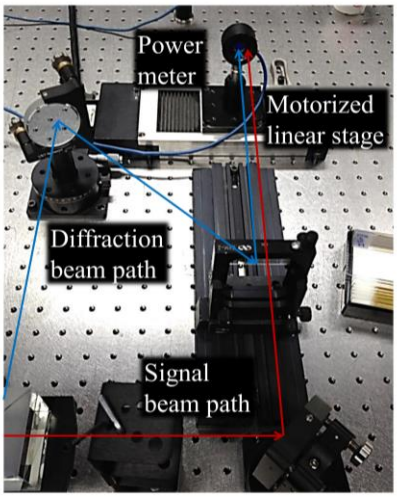

(a)

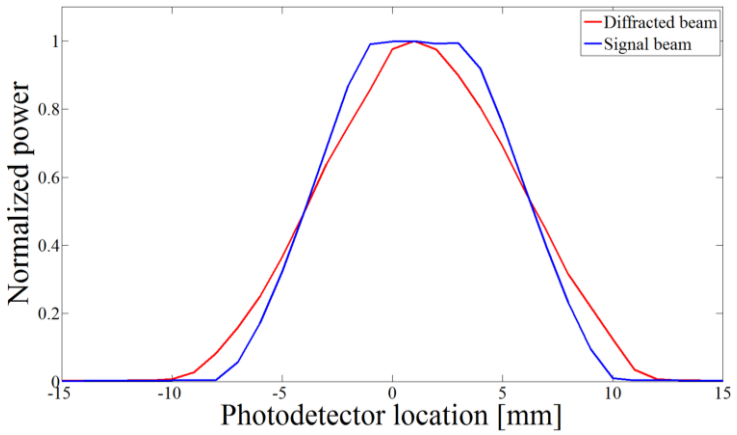

(b)

Figure 2.10 Experiment for measuring the shrinkage on the photopolymer along the length direction: (a) a captured image of the experimental setup and (b) measured data for both the reconstructed and signal beams.

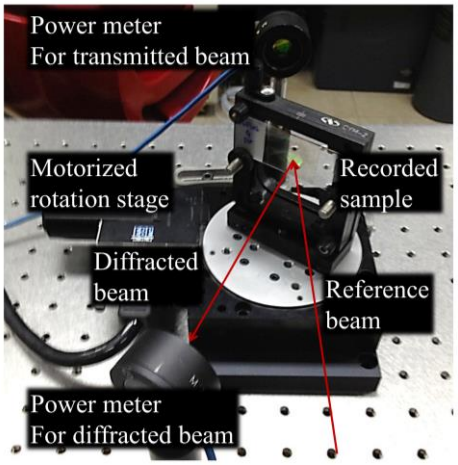

(a)

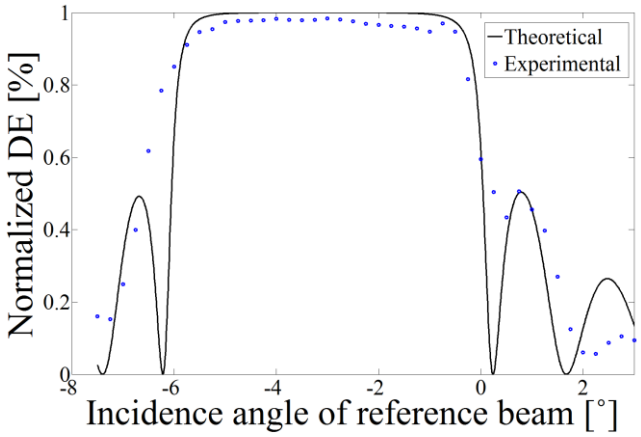

(b)

Figure 2.11 Experiments for measuring the shrinkage on the photopolymer along the thickness direction: (a) a captured image of the experimental setup and (b) the measured Bragg curve (dots) of diffraction efficiency (DE) overlaid on the best-fit curve (solid line) calculated by coupled wave theory.

wave theory [55] with the volume grating vectors which have varying α_d. Figure 2.11(b) shows the measured Bragg curve (dots) along with the best-fit curve (solid line) by the coupled wave theory. The best-fit curve is calculated from the coupled wave theory using the volume grating vector which has α_d=0.0198. From this result, it is confirmed that the photopolymer used in the experiments has 1.98 % shrinkage along the thickness direction.

2.5 Results

The photopolymer film is chosen for the holographic material in the experiments performed in this dissertation work. The photopolymer film has the beneficial characteristics compared to the other holographic materials used for the holographic recording, such as high diffraction efficiency, capability of wavelength multiplexing, easiness of handling, transparency after hologram recording, and so on. Principle of index modulation in the photopolymer is described by using the polymerization chemical process. It modulates the refractive index by the index differences between the photo-reacted polymerized parts and the base matrix material.

The photopolymer film used in the experiments has more than three different photo-initiators to make it possible to do full-color hologram recording on the film. Three reflection holograms are recorded on the photopolymer film, using red (671 nm), green (532 nm), and blue (473 nm) lasers, to evaluate the dosage responses at the three primary colors. From the three dosage curves measured at the wavelengths of primary colors, nearly 100 % of diffraction efficiencies are observed at all of the three wavelengths. In addition, the wavelength multiplexing on the photopolymer film for the full-color recording is also examined by the experiments. When the proper

exposure condition is satisfied in the wavelength multiplexing recording procedure, similar diffraction efficiencies of around 50 % at the three wavelengths of primary colors are measured from the wavelength multiplexed hologram recorded on the photopolymer film. Display experiments are performed to evaluate the wavelength multiplexing and see-through properties of the photopolymer film. From the resultant images in the display experiments, it is clearly confirmed that the photopolymer film is suitable for the holographic recording techniques for displaying full-color images with see-through property.

Furthermore, the shrinkage characteristics, one of the disadvantages of the photopolymer film, are theoretically analyzed, and the amount of shrinkage along the thickness and length directions are measured by the experiments. The shrinkages along the length and thickness directions affect the direction of the reconstructed wave and the diffraction efficiency, respectively. The measured values of shrinkages on the photopolymer film used in the experiments are 0 % and 2.6 % for the length and thickness directions, respectively. Since the shrinkage on the length direction is negligible, the hologram recorded on the photopolymer can be reconstructed without any angular shift and color separation.

Chapter 3 High resolution autostereoscopic 3D display using holographic printing

3.1 Introduction

The holographic stereogram is one of the prominent methods for displaying autostereoscopic 3D images [56]. In this technique, 3D images are synthesized from sequences of closely spaced 2D perspective views and are discretely recorded as a hologram on a holographic material like photopolymer. These series of 2D perspective images are stored in small holographic elements, called hogels [57]. With an appropriate illumination, each hogel in the holographic stereogram diffracts a fraction of perspective images within a certain viewing angle. The diffracted lights are fractions of the perspective image recorded on the hogels in the holographic stereogram. On the observing plane, relatively large numbers of viewing points are formed by the merged lights diffracted from the hogels. An observer can see

a 3D image from these perspective views at the corresponding viewing point. When the observer's left and right eyes are located at different viewing points, the observer sees stereoscopic images and perceives 3D images [58].

In this chapter, the principle and previous research of a holographic printer, which is a holographic recording method for implementing the holographic stereogram, are introduced first. And then, a novel hogel overlapping method is presented to enhance the resolution of the holographic printer. Computer simulations of the hogel recording in the holographic printer are performed to explain why the recordable hogel size cannot be reduced infinitesimally. The proposed method assumes that the holographic printer using photopolymer as a holographic material can record hogels as a volume hologram. According to the volume hologram theory, multiple holograms can be superimposed by several multiplexing methods including angle, wavelength, space, and so on [59, 60]. With the multiplexing property of the photopolymer, the proposed method can increase the lateral resolution by recording spatially multiplexed hogels with overlap to avoid decreasing the hogel size. In addition, the lateral resolutions of the two holographic stereograms, which are optically recorded by the conventional and proposed methods, are presented to demonstrate the validity of the proposed hogel overlapping method for the holographic printer.

3.2 Overview of holographic printing method

The holographic stereogram is composed of a large number of hogels. To build a large number of hogels on the holographic material, the holographic printer sequentially records the hogels until the whole area of the holographic material is recorded like a conventional dot printer. Figure 3.1 illustrates the principle of a reflection-type holographic printer. For a signal beam, the perspective object images displayed on an SLM are illuminated by an expanded laser beam and converged on the surface of the holographic material with a predefined area. This predefined area determines the size of the hogel as *p*. A reference laser beam is incident on the same area from the opposite side to generate the reflection hologram. The information about the perspective images on the SLM is recoded as an interference pattern formed by the signal and reference beams in the hogel.

After a single hogel is recorded, a motorized two-axis linear stage translates the holographic material horizontally and vertically to the next recording position, and consecutive perspective images are displayed on the SLM for the next hogel recording. The distance of translations, or shifting distance, along the horizontal and vertical directions of the motorized stage is indicated as δ in Fig. 3.1. In the conventional holographic printer, in general,

translations of the holographic material (δ) are equal to the size of the hogel (p). The recording characteristics of the hogel are closely related to the quality of 3D images in the holographic stereogram. For example, viewing image qualities, such as lateral and angular resolutions, color representation, viewing angle, are directly affected by the characteristics of hogels. Each hogel should provide a homogenous spectrum to provide a natural 3D image, and the size of the hogel is directly related to the lateral resolution of the holographic stereogram [57]. In view of the importance of hogels in the holographic stereogram, methods for recording hogels in holographic printing have been actively studied in recent years in both academic and commercial fields [61-70]. Yamaguchi *et al*. reported a holographic printer using an SLM for exposing perspective images to the corresponding hogels in 1990s [61-64]. Peyghambarian group worked on rewritable holographic printing by using a photorefractive polymer as holographic material [65-67]. Some holographic printers have been used commercially by several companies like Zebra Imaging and Geola. Zebra Imaging commercialized a full-color and large format holographic printer [68, 69], and Geola proposed a fast recordable holographic printer using a pulsed laser and reported an even faster printing method using a hologram copier [70-72].

Figure 3.2 shows commercially available holographic printers

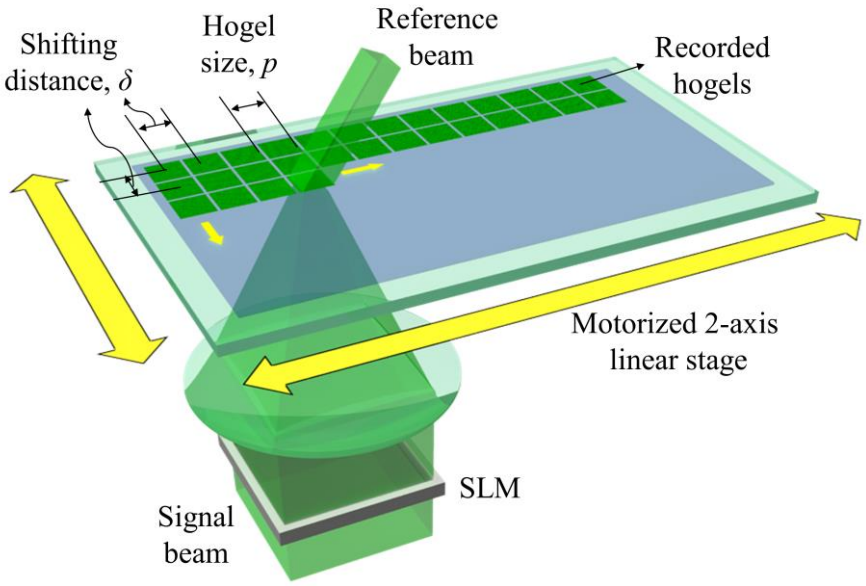

Figure 3.1 Schematic diagram of the holographic printer.

manufactured by Geola and Zebra Imaging, and the specifications of these holographic printers are listed in Table 3.1. Even though these holographic printers use different recording materials, which are silver halide and photopolymer in Geola and Zebra Imaging respectively, both products provide large recordable size and a wide field of view for commercial uses. A noticeable specification of both holographic printers is the minimum size of recordable hogel. The minimum hogel sizes of Geola's and Zebra Imaging's holographic printer are 0.4 and 0.71 mm, respectively. These minimum hogel sizes are relatively large compared to typical display devices like FPDs. Though the lateral resolution of the holographic printer is an important quality factor, the enhancement of lateral resolution, or decreasing the size of hogel, has not been actively investigated as the examples of the commercial holographic printers.

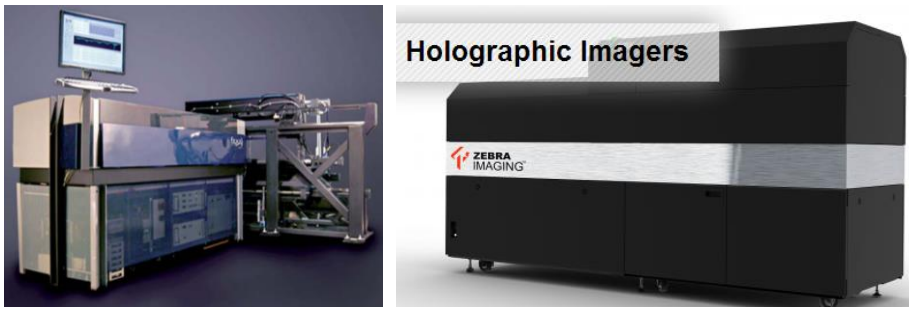

(a) (b)

Figure 3.2 Commercially available holographic printers manufactured by (a) Geola and (b) Zebra Imaging.

Table 3.1 Specifications of commercially available holographic printers

	Geola	Zebra Imaging
Recording material	Silver halide	Photopolymer
Hogel size	0.4-2 mm	0.71 mm
Recordable size	800 × 800 mm	600 × 850 mm
Field of view	105˚	90˚

3.3 Limitation on enhancing lateral resolution of holographic printing

The lateral resolution of the holographic printer can be increased by decreasing the hogel size, because it is inversely proportional to the hogel size. However, the size of hogel cannot decrease infinitesimally owing to the recording principle of the holographic printer. Figure 3.3 shows an optical arrangement on the signal beam path in the holographic printer to explain the recording principle. The perspective image on the SLM is Fourier transformed by a lens to the Fourier plane where the hogel mask is located. After passing the hogel mask, the signal beam is then demagnified and relayed through 4-*f* optics to the holographic material of photopolymer. On the plane of the holographic material, the relayed signal beam is interfered with the incident reference beam from the opposite side, and the information on the SLM is recorded on the holographic material with the resultant interference pattern.

Although the hogel mask is designed to set the size and shape of the hogel, it also plays a role of a spatial filter due to its position on the Fourier plane. The hogel mask performs as a high-frequency cutoff spatial filter, and blocks the high-frequency components of the image on the SLM. As a result,

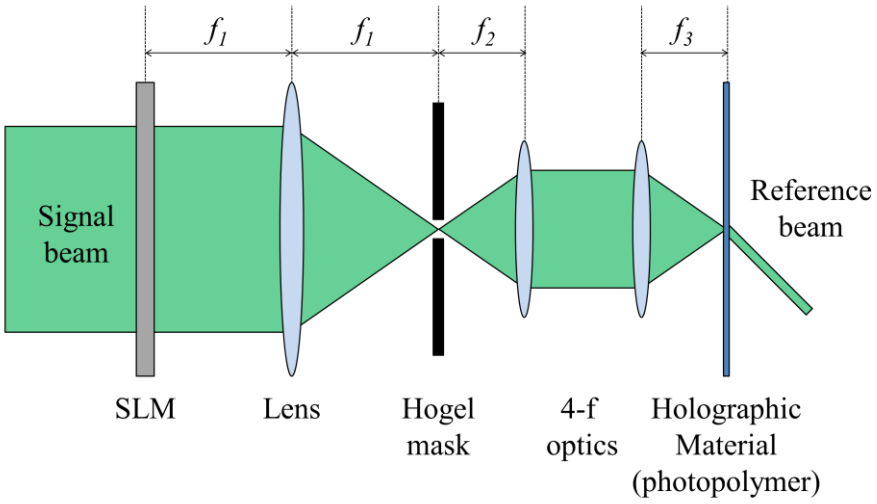

Figure 3.3 An optical arrangement on the signal beam path of the holographic printer.

if the hogel mask is too small, the perspective image on the SLM cannot be perfectly transferred to the holographic material, and thus a blurred image is recorded. For this reason, the recording small-sized hogel for a high lateral resolution of the holographic stereogram causes loss of high-frequency components of the perspective image, which means a quality degradation of the recorded image.

In order to find out an impact of the size of hogel mask on the quality of the image reconstructed on the holographic stereogram, a computer simulation of an image transformation from the SLM to the holographic material has been performed. In this computer simulation, the hogel mask is assumed as a perfect square which has the length of a side *W*. Then, the hogel mask function *H* is expressed in coordinates (*u*, *v*) on the Fourier plane with a rectangular function *rect*

$$H(u,v) = rect\left(\frac{u}{W}\right) rect\left(\frac{v}{W}\right). \tag{3.1}$$

The input image I_{in} on the SLM in coordinates (*x*, *y*) is Fourier transformed on the Fourier plane by the first lens in front of the SLM. The spatial filtering of the hogel mask on the Fourier plane can be expressed by multiplying the Fourier transformed input image by the hogel mask function. In order to visualize the degradation on the reconstructed hogel image due to

the size of hogel mask, the spatially-filtered Fourier transformed input perspective image is reconstructed by the inverse Fourier transform. The reconstructed perspective image I_{re} is represented by

$$I_{re}(x,y) = F^{-1}(F(I_{in}(x,y)) \times H(f_X \lambda f, f_Y \lambda f)), \qquad (3.2)$$

where F and F^{-1} are the Fourier transform and the inverse Fourier transform, respectively. Note that the amplitude and phase of the light on the Fourier plane are determined by those of the input Fourier component at frequencies f_X and f_Y, where $f_X = u/\lambda f$ and $f_Y = v/\lambda f$ for the wavelength λ [73].

In the computer simulation, SLM has a 720 x 720 lateral resolution with a 14 μm pixel pitch, and the focal lengths for the first lens (f_1) and the 4-f optics (f_2 and f_3) are 150 mm, 75 mm, and 4 mm, respectively. The specifications of the SLM and lenses assumed on the computer simulation are the same as those used in the experiments explained in Section 3.5. We measured the peak signal to noise ratio (PSNR) between the input image (I_{in}) displayed on the SLM and the reconstructed perspective image (I_{re}) by varying the size of the hogel mask from 0 mm to 8 mm at intervals of 0.1 mm. The actual hogel sizes recorded on the holographic material plane are 0 μm to 427 μm, resulted from the demagnification in the 4-f optics.

The USAF resolution chart is used for the input image on the SLM

which has a resolution of 720×720 as shown in Fig. 3.4(a). The reconstructed hogel images for the hogel sizes of 100 μm, 200 μm, and 400 μm are shown in Figs. 3.4(b), respectively. The graph in Fig. 3.4(c) illustrates the dependency of PSNR on the size of hogel mask, which indicates the PSNR decrease with reducing the size of recorded hogel. The numerical values of PNSR are 40.79 dB, 47.87 dB, and 55.12 dB for the hogel images reconstructed with hogel sizes of 100 μm, 200μm, and 400 μm, respectively. As expected, the reconstructed hogel images show quality degradation, such as image blur, and the degradation is getting worse when the size of hogel mask decreases.

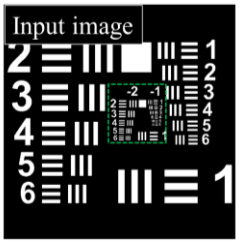

(a)

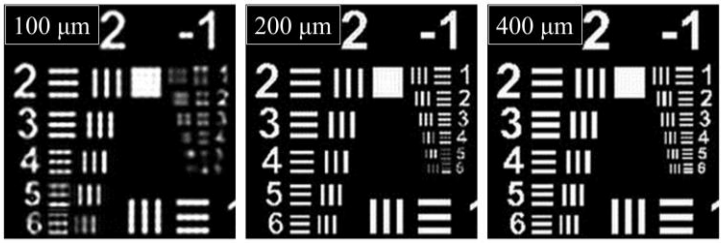

(b)

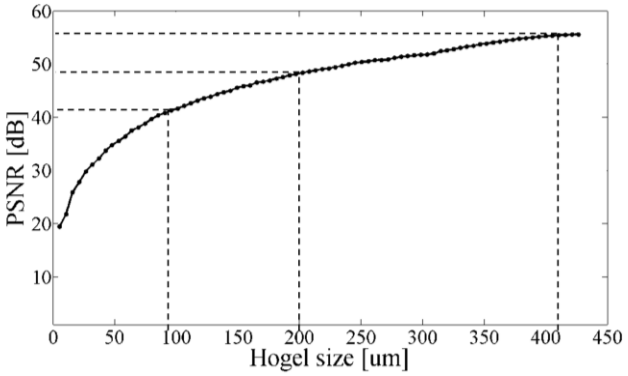

(c)

Figure 3.4 Degradation of the image quality for the reconstructed hogel images by decreasing the size of the recorded hogel: (a) input image on the SLM, (b) reconstructed hogel images for the recorded hogel sizes of 100 μm, 200 μm, and 400 μm, and (c) the dependency of PSNR on the hogel size in a range of 0 μm to 427 μm.

3.4 Hogel overlapping method for enhancing lateral resolution of holographic printer

Volume holographic multiplexing techniques are employed to enhance the lateral resolutions of the holographic printer without image degradation due to its small hogel size. Since the photopolymer is used as the holographic material for the volume hologram, every perspective image in the hogels is recorded as a volume hologram. Bragg selectivity property of the volume hologram allows multiple holograms to be recorded in the same area of the holographic material [26].

The hogel is the smallest addressable element in the holographic stereogram, and the interval among the hogels, shifting distance in the holographic printer, is inversely proportional to the lateral resolution of the holographic stereogram. Since the shifting distance δ is equal to the hogel size p in the conventional holographic printer, the lateral resolution of the conventional holographic printer is decided by the hogel size. As explained in the previous section, however, the hogel size cannot be arranged to be infinitesimally small for increasing the lateral resolution.

In this chapter a hogel overlapping method for the holographic printer is presented in order to improve the lateral resolution while maintaining a

constant hogel size. In the proposed hogel overlapping method, the shifting distance is smaller than the hogel size, which makes adjacent hogels overlapped. When the hogel is a perfect square and the shifting distances in vertical and horizontal directions are equal, the maximum number M of overlapped hogels is expressed as

$$M = 2\left\lceil \frac{p}{\delta} \right\rceil, \tag{3.3}$$

where $\lceil \alpha \rceil$ denotes the smallest integer not less than α.

The maximum number of recordable overlapped hogels depends on the dynamic range of holographic material used in holographic printing. The dynamic range of holographic material is a measure of the capacity of the media, i.e., how many holograms can be stored at a given diffraction efficiency. And it is determined by the maximum refractive index modulation and the thickness of holographic material [74].

To get a uniform image, the ratio (α) of p to δ should be a natural number so that the overall hogel has identically overlapped except for the hogels at the edges. When this condition is satisfied, the lateral resolution of the proposed hogel overlapping method can be uniformly increased by a factor of α^2.

Figure 3.5 illustrates a typical example of recording schemes for the

conventional holographic printing method (M=1 and α=1) and the proposed hogel overlapping method (M=4 and α=2). In this figure, a dashed box and dots in it represent the recorded hogel and the center points of recorded hogels, respectively. Both methods have the same hogel size of 400 μm. In contrast to the conventional method which has the shifting distance identical to the hogel size, the proposed new method has a shifting distance of 200 μm which is a half of the hogel size. Though the overlap region exists in four adjacent hogels in the proposed method, image information on each of four perspective images can be recorded on the same area of the photopolymer thanks to the multiplexing property of the volume hologram. In this example, the proposed method has a lateral resolution enhanced by 4 times compared to the conventional method.

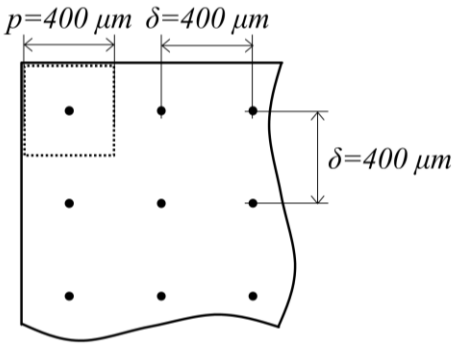

(a)

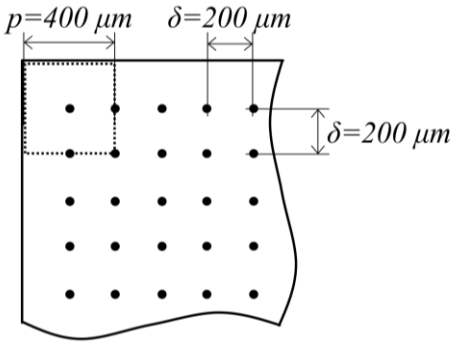

(b)

Figure 3.5 Graphical descriptions for recorded hogels (a) in a conventional scheme (M=1 and α=1) and (b) in a proposed hogel overlapping scheme (M=4 and α=2).

3.5 Experiments

An experimental setup for holographic printing has been built up to verify the resolution enhancement by the proposed method. Figure 3.6 shows a schematic diagram of the experimental setup of holographic printer system. A DPSS green (532 nm) laser is used for a light source, and an electric shutter is used to control the time of a light exposure. The polarization state of the laser is adjusted by a pair of a λ/2 wave-plate and a polarizer. After a beam is expanded by a spatial filter and a 50 mm focal length collimating lens (L1), a power ratio of the signal to reference beam is adjusted by a λ/2 wave-plate, a polarizing beam splitter, and polarizers. On the signal beam path, a series of perspective images are loaded on the SLM with a diffuser, and focused on the photopolymer by an objective lens (OL2) with 4-*f* relay lenses (L2 and L3) whose focal lengths are 150 mm and 75 mm, respectively. The SLM used in the experimental setup is a transparent liquid crystal (LC) display which has a 1280×720 resolution with a 14 μm pixel pitch. The displayed perspective image on the SLM has a resolution of 720×720 pixels. The reference beam is incident on the photopolymer through two 250 mm focal length lenses (L4 and L5) with an incidence angle of 60°. To record rectangle-shaped hogels on the photopolymer, hogel masks are located on

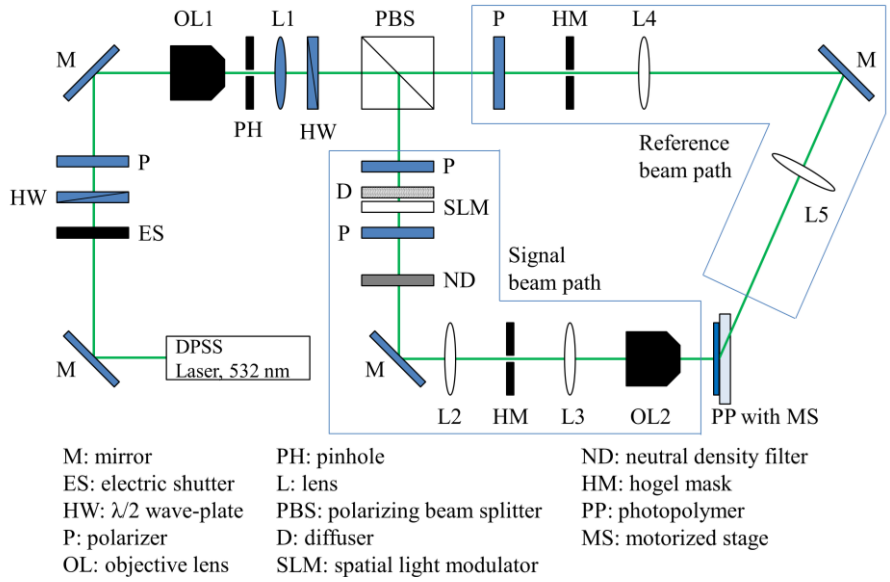

Figure 3.6 A schematic diagram of the experimental setup for the holographic printer system.

both signal and reference beam paths. In the intersection of signal and reference beams, a photopolymer is located on a motorized two-axis linear stage. The linear stage has a 0.25 μm precision and a 205 mm travel range on both horizontal and vertical directions. The photograph of the experimental setup for holographic printing is shown in Fig. 3.7.

Two holographic stereograms are recorded to compare the lateral resolutions between the conventional and proposed holographic printing methods as described in Fig. 3.5 and Table 3.2. For the perspective images, the computer generated perspective images are used. Those have information of a scene of two objects, a cube and a sphere, located in different depths. To record their holographic stereograms in the same area for both methods, 50×50 and 100×100 perspective images are printed in hogels for the conventional and proposed method, respectively. Compared to the conventional method, total number of hogels in the proposed method is four times larger than that in the conventional method, which means that the lateral resolution of the proposed method is increased by four times.

The resultant holographic stereograms captured from four different viewing points for the conventional and proposed methods specified in Table 3.2 are compared in Fig. 3.8. Both holographic stereograms in Fig. 3.8, are captured from right, left, top, and bottom viewing points, and the captured

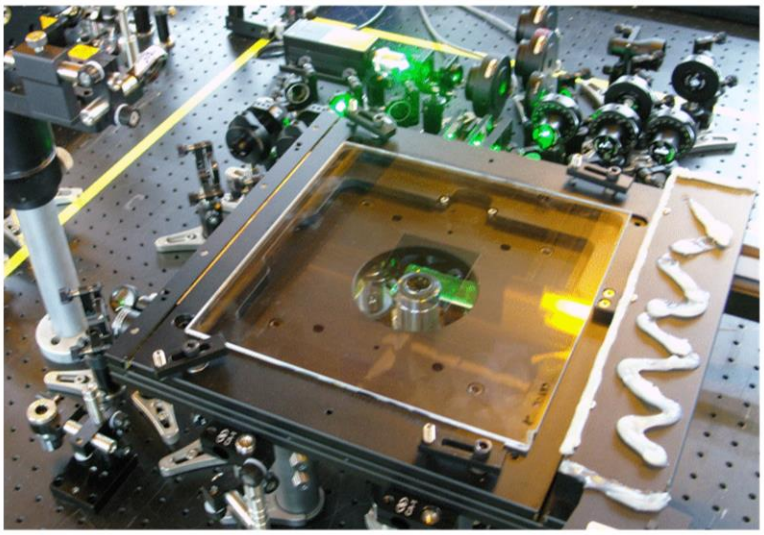

Figure 3.7 Photograph of the holographic printer system used for the experiments.

Table 3.2 Parameter values used in the experiments for the conventional and proposed holographic printing methods

	Conventional method	Proposed method
Hogel size (p)	400 μm	400 μm
Shifting distance (δ)	400 μm	200 μm
Number of hogels	50 × 50	100 × 100

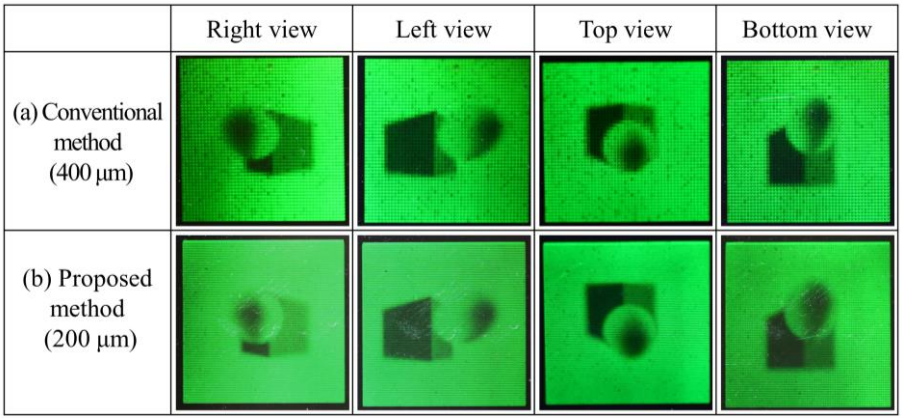

Figure 3.8 Perspective images of reconstructed holographic stereograms captured from different viewing points: (a) conventional method and (b) proposed method.

images are focused on the photopolymer plane. It is clearly confirmed in the experiments that the captured holographic stereogram images using the proposed hogel overlapping method have much higher lateral resolution compared to the images captured from the conventional method. Also the holographic stereograms captured at different focuses for the conventional and proposed methods are compared in Fig. 3.9. Each holographic stereogram is captured at the focus of the photopolymer plane, object ‘cube’, and ‘sphere’. Edges of the object ‘cube’ and ‘sphere’ are much clearly observed in the captured holographic stereograms using the proposed method (Figs. 3.9(d)-(f)) compared to those implemented by the conventional method (Figs. 3.9(a)-(c)). The experimental results shown in Figs. 3.8 and 3.9 support the validity of the proposed method of hogel overlapping holographic printing for the enhancement of the lateral resolution.

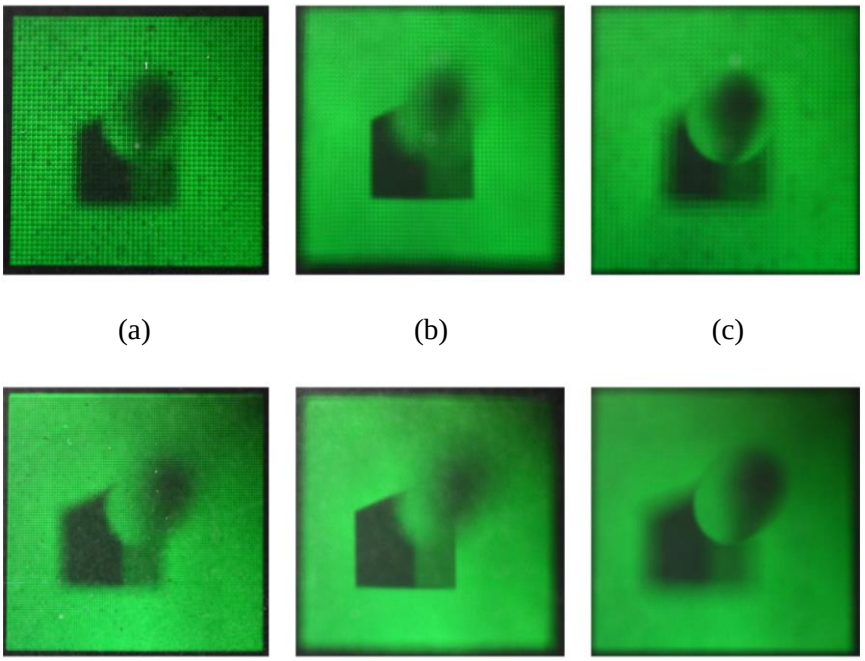

(a) (b) (c)

(d) (e) (f)

Figure 3.9 Stereoscopic stereograms captured at different focuses of the photopolymer ((a) and (d)), object ‘cube’ ((b) and (e)), and object ‘sphere’ ((c) and (f)). Holographic stereograms in (a)-(c) and (d)-(f) are printed by the conventional and proposed hogel overlapping methods, respectively.

3.6 Results

In this section, a novel method for enhancing the lateral resolution of holographic stereogram is proposed by hogel overlapping in the holographic printer. Since the high-frequency components of perspective images are lost when the size of hogel is decreased, the enhancement of the lateral resolution by decreasing hogel size has limitations. By taking advantage of multiplexing property of the volume hologram, hogels can be recorded in the overlapped region. When we record hogels in the overlapped region, the interval among hogels is smaller than the size of hogel, and thus the lateral resolution of holographic stereogram can be enhanced. The maximum number of overlapped hogels is discussed in conjunction with the dynamic range of the holographic material. The holographic printing system is built, and it can control the shifting distance by the motorized two-axis linear stage. Comparison of the two holographic stereograms, optically recorded by using conventional and proposed holographic printing methods, reveals the feasibility of the lateral resolution enhancement by the proposed method. The perspective images from different viewing points are demonstrated to compare the lateral resolutions between two holographic stereograms. The experimental results for the proposed hogel overlapping holographic

stereogram confirm the enhancement of lateral resolution compared to the conventional holographic stereogram.

Chapter 4 See-through autostereoscopic 3D display using lens-array holographic optical elements

4.1 Introduction

Augmented reality (AR) is a technology that aims to provide a virtual image overlaid or superimposed onto a real world scene through a display device [75]. AR has been actively studied so far and shown significant advancement in its research lately by virtue of the development of mobile device, computer vision science, and display technologies [75-78, 4]. There are two ways to display virtual images in the AR by using a monitor based display or an optical see-through display [76]. In the monitor based AR, sight of a user is blocked by the display device and both the real world scene and the virtual image are provided by the display device. On the other hand, in the optical see-through AR, the user can perceive the real world scene directly through the AR system while virtual images are overlaid on the physical world by a

transparent screen or display. Since the optical see-through AR does not have drawbacks such as a low resolution of reality scene and a user disorientation compared to the monitor based AR, it has been spotlighted more than the monitor based AR recently as in the case of *Google Glass*.

In spite of these recent interests and active research in the optical see-through AR, most of reported optical see-through AR systems provide 2D virtual images only, being unable to display 3D virtual images. However, several research groups have recently presented optical see-through AR systems supporting 3D virtual images [79-85]. To provide 3D virtual images in an optical see-through AR system, Takaki *et al*. adopted a super multi-view (SMV) scheme [81, 83], and Hong *et al*. used an integral floating display [82] as shown in Fig 4.1(a) and (b), respectively. However, the former needs an imaging device of excessively high resolution to satisfy the SMV condition, and the latter requires complicated fabrication procedures to produce an image combiner. Furthermore, since both the methods basically adopt conventional autostereoscopic 3D displays, they need additional optical systems in front of the imaging devices, and consequentially the total systems based on both methods are unavoidably bulky.

Holographic recording techniques can be adopted for realizing autostereoscopic 3D see-through AR systems. However, the holographic

(a)

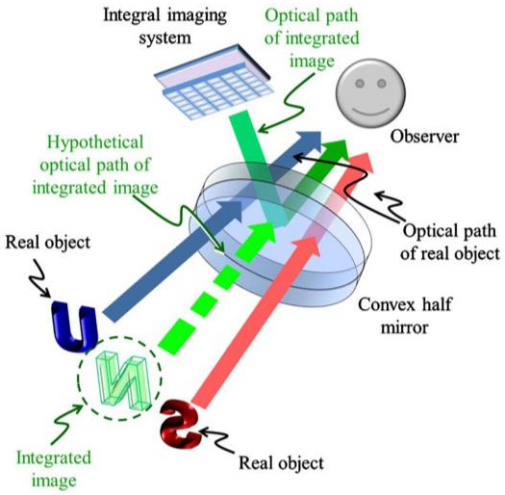

(b)

Figure 4.1 Previous research on autostereoscopic 3D see-through AR systems by adopting (a) super multi-view display [81] and (b) integral floating display [82].

stereogram introduced in the previous chapter can only present a static autostereoscopic 3D image because the perspective images for one stationary 3D scene are recorded on it in the form of the hogels. One possible reported method to display dynamic images on the holographic stereogram is using the rewritable photorefractive polymer for the holographic material in the holographic recording procedure [67]. However, so far, the photorefractive polymer stays in a quasi-real-time dynamic status. It is hard to realize high frame-rate autostereoscopic 3D image by the holographic stereogram, and it is not proper to the AR system. The HOE is an alternative for the image combiner which can display the autostereoscopic 3D images in the optical see-through AR. HOE is a hologram that consists of diffraction gratings which have optical functions of conventional optical elements, such as mirrors, lenses, and so on. The image combiner of HOE satisfies the see-through property without loss of brightness of real world scenes, which is essential for the optical see-through AR, because the HOE functions as the image combiner just for the Bragg matched lights [22]. The image combiner using HOE also has the advantages of narrow thickness and low cost. Furthermore, it has capability for displaying dynamic images because HOE itself performs as optical elements and images can be modulated from an external spatial light modulator such as an image projector.

4.2 Full-color lens-array holographic optical elements for displaying integral images

In this section, a novel full-color autostereoscopic 3D display is presented which is based on a projection-type integral imaging [82] for the optical see-through AR by making use of a full-color lens-array HOE as the image combiner. Principles of the lens-array HOE are introduced first, and then a recording scheme for the HOE having full-color and lens-array functions is described. Lastly, feasibility of the proposed system for displaying virtual 3D images in the optical see-through AR is verified by the experiments.

4.2.1 Principles of full-color lens-array holographic optical elements

In the proposed AR system, the lens-array HOE plays a role of the image combiner for displaying autostereoscopic 3D images. Principles of the lens-array HOE from recording and reconstruction perspectives are depicted in Figs. 4.2(a) and (b), respectively. In the recording scheme of the volume hologram, an interference pattern formed by the plane wave reference beam and the spherical wave signal beam, containing properties of the conventional lens-array, is recorded into the holographic material in the form

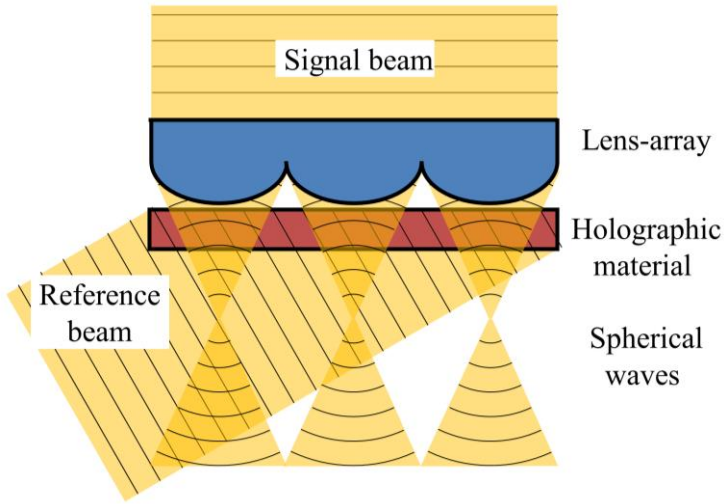

(a)

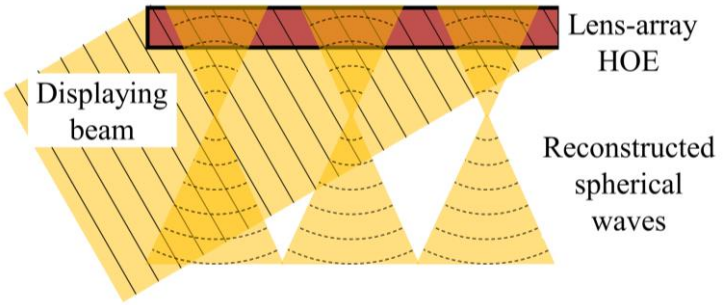

(b)

Figure 4.2 Principles of (a) recording and (b) displaying for the lens-array HOE.

of a lens-array HOE. The recorded lens-array HOE reconstructs the duplicated wavefronts of the conventional lens-array when a displaying beam, identical to the reference beam in the recording scheme, is projected on the lens-array HOE.

The photopolymer film is used for the holographic material in this work because it has the advantage of wavelength multiplexing for a full-color recording, and has an optically clear characteristic for the see-through property after hologram recording [86]. The photopolymer used in the experiments are provided from Bayer MaterialScience AG and the thickness of the photopolymer is 14-18 um.

As the image combiner, the proposed lens-array HOE recorded on the photopolymer can provide the virtual 3D images with the see-through condition nicely satisfied. As the lens-array HOE modulates only Bragg matched lights from the imaging device, Bragg mismatched lights from the real world just pass through the lens-array HOE without feeling it as an optical element. Furthermore, to provide more realistic virtual images on the proposed AR system, the wavelength and spatial multiplexing techniques [26] are adopted in the recording procedure to display full-color virtual images and to record a large sized lens-array HOE, respectively.

4.2.2 Hologram recording setup for fabricating proposed lens-array holographic optical elements

Figure 4.3(a) illustrates a schematic diagram of the experimental setup for recording the full-color lens-array HOE, and Fig. 4.3(b) shows a photograph of its experimental setup. The three laser beams of red (671 nm), green (532 nm), and blue (473 nm) are combined into a single beam path in a beam combining part. The $\lambda/2$ wave plates located in the beam paths of the three lasers control the states of polarization. The power densities of the three lasers are adjusted by circular variable neutral density filters, and the exposure time of the combined single beam is determined by an electric shutter. The combined laser beam is expanded into a collimated plane wave by a spatial filter and a collimating lens in a beam expanding part. In a recording part, the expanded beam is divided into the reference and signal beam paths through a beam splitter. Since the reflection hologram is preferable for wavelength multiplexing, the two beam paths are arranged to be incident on the photopolymer in opposite directions. A lens-array with 1 mm lens pitch and 3.3 mm focal length is located in the signal beam path, and the photopolymer mounted on a motorized stage is located at an intersecting position of the reference and signal beam paths. The signal beam

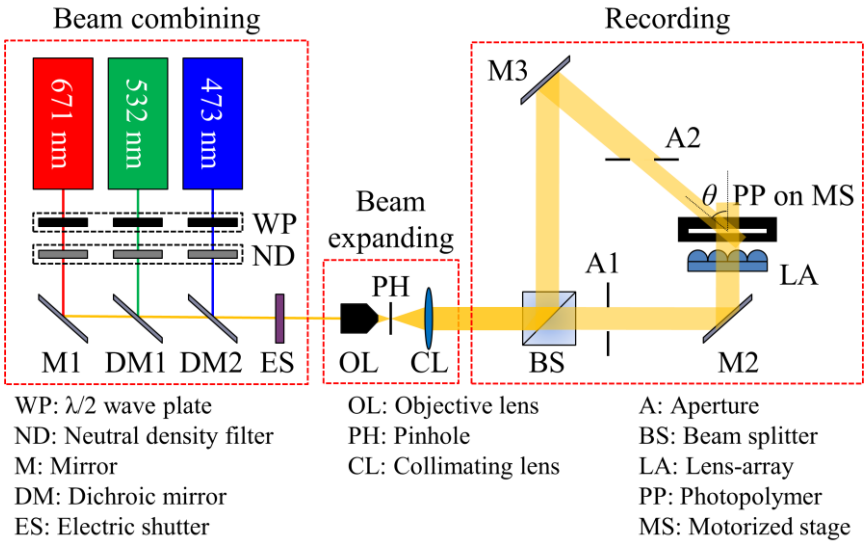

(a)

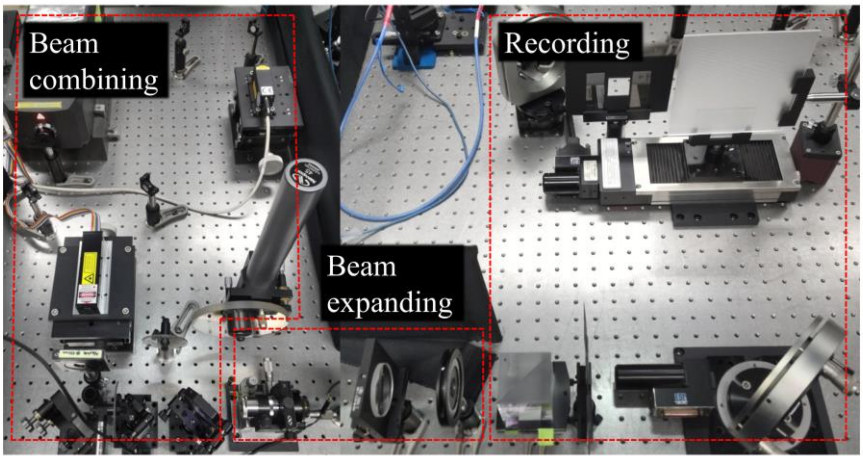

(b)

Figure 4.3 Experimental setup for recording the full-color lens-array HOE: (a) schematic diagram and (b) photograph of its optical arrangement.

is incident normally to the photopolymer, while the reference beam is projected with an incidence angle (θ) of 50˚. Two square apertures with a side length of 30 mm are located in both beam paths for a precise alignment of the exposed area on the photopolymer. The size of recordable area on a fixed photopolymer is limited by the size of the square apertures. In order to enlarge the total recordable size of the photopolymer, a one-axis motorized linear stage is used for spatial multiplexing. In this setup, a 30 mm × 60 mm lens-array HOE is recorded by the spatial multiplexing with 30 mm horizontal translation of the one-axis motorized linear stage. The exposure condition should be optimized for achieving similar magnitudes of diffraction efficiencies for the three wavelengths. To optimize the exposure condition, the three lasers are exposed on the photopolymer simultaneously, while varying the power densities of the lasers individually. The full-color lens-array HOE to be used in the next displaying experiments is recorded on the exposure conditions of 51 mJ/cm^2 for 473 nm, 59 mJ/cm^2 for 532 nm, and 47 mJ/cm^2 for 671 nm.

When the collimated reference light is projected, the full-color lens-array HOE reconstructs highly diverging diffracted light because it has a short focal length. Due to the highly diverging diffracted lights of the lens-array HOE, in the reflection hologram geometry, it is very difficult to

directly measure the diffraction efficiency of the reconstructed lights. Instead of direct measuring of the diffracted light, alternatively, transmittance and reflectance spectrums of the full-color lens-array HOE are measured to calculate the diffraction efficiencies within the visible range of the spectrum [87]. Furthermore, diffraction efficiencies of the three primary colors recorded in the full-color lens-array HOE can be simultaneously measured when the spectrum based method is used for measuring diffraction efficiencies.

Since an image projector which has a broadband incoherent light source is used to modulate and project images on the full-color lens-array HOE, a spectrometer (Ocean Optics, USB4000-VIS-NIR) with an incoherent white light source (Ocean Optics, HL-2000-FHSA) is used for measuring transmittance and reflectance spectra of the full-color lens-array HOE. When absorption and scattering in the photopolymer are negligible, the diffraction efficiency (*DE*) can be obtained by

$$DE = 100 - T - R, \tag{4.1}$$

where T is the transmittance and R is the reflectance of the recorded full-color lens-array HOE, as described in the inset of Fig. 4.4.

The transmittance (*T)* and reflectance (*R*) are observed by the

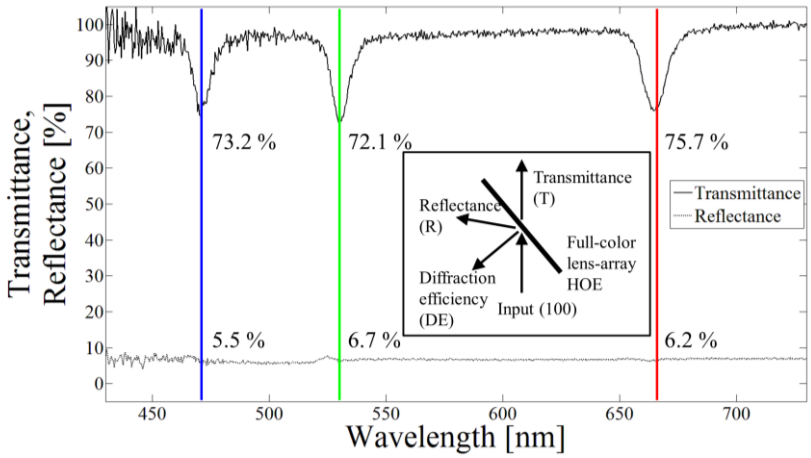

Figure 4.4 Transmittance and reflectance of the recorded full-color lens-array HOE measured in the displaying experiments according to wavelengths. The inset describes the beam paths on the HOE for measuring the diffraction efficiency.

Table 4.1 Measured values of transmittance, reflectance, and diffraction efficiency for red, green, and blue color three laser beams displayed by the recorded full-color lens-array HOE.

	Red	Green	Blue
Transmittance (*T*)	75.7 %	72.1 %	73.2 %
Reflectance (*R*)	6.2 %	6.7 %	5.5 %
Diffraction efficiency (*DE*)	18.1 %	21.2 %	21.3 %

spectrometer in the displaying experiments, and their measured curves are plotted along the wavelength in Fig. 4.4. The measured values of transmittance (*T*), reflectance (*R*), and *DE* for red, green, blue colors are listed in Table 4.1. Displaying the recorded full-color lens-array HOE results in the similar values of *DE*: 18.1 %, 21.2 %, and 21.3 % for red, green, and blue colors, respectively.

4.2.3 Three-dimensional imaging on full-color lens-array holographic optical elements

Figure 4.5(a) shows a photograph of the experimental setup for displaying 3D virtual images in an optical see-through AR system using the proposed full-color lens-array HOE. A beam projector is used for an imaging device. Since the collimated reference beam is used in the recording setup, the imaging device for a displaying setup should also project a collimated light on the full-color lens-array HOE to avoid the Bragg mismatch. To project the collimated images on the full-color lens-array HOE, a telecentric lens is used with the relay optics. However, if a diverging reference beam is used in the recording setup, the telecentric lens is not necessary, and a diverging angle of the projected image can be controlled by the relay optics. The full-color lens-

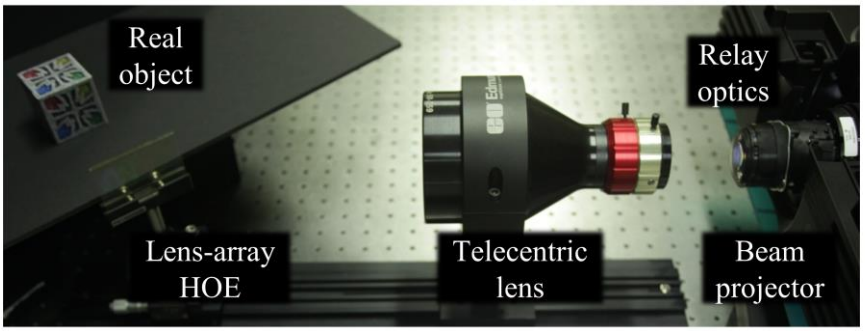

(a)

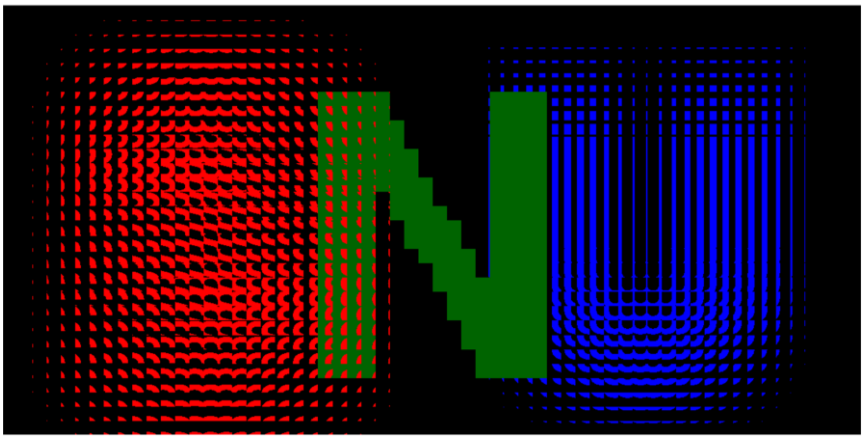

(b)

Figure 4.5 (a) Experimental setup for displaying 3D virtual images in the proposed optical see-through AR system, and (b) the elemental images for three characters (‘S’, ‘N’, and ‘U’) projected on the lens-array HOE for 3D virtual imaging.

array HOE is located in the path of the collimated light with the incidence angle of 50˚ which is identical to that of the reference beam in the recording setup. To illustrate the see-through property of the proposed AR system, a real object 'cube' is located behind the full-color lens-array HOE.

As the projection-type integral imaging is employed in the proposed method, elemental images should be projected on the full-color lens-array HOE to generate the autostereoscopic 3D virtual images [88]. The computer-generated elemental images are projected on the lens-array HOE. It has 3D information of three characters, 'S', 'N', and 'U', as shown in Fig. 4.5(b). To demonstrate the color representation and the 3D imaging of the proposed system, each character of 'S', 'N', and 'U' in the elemental images has both the color information of red, green, and blue, and the depth information of +30 mm, 0 mm, and -30 mm, respectively.

Figure 4.6 shows the resultant see-through 3D virtual images captured in the displaying experiments from five different viewing points relative to the proposed optical see-through AR system. It is clearly confirmed in the experiments that the different perspective images captured from left, right, top, and bottom viewing points provide proper disparities among three letters, 'S', 'N', and 'U'. The disparities among the virtual images shown in Fig. 4.6 provide a binocular disparity and give a 3D perception to the observers [7].

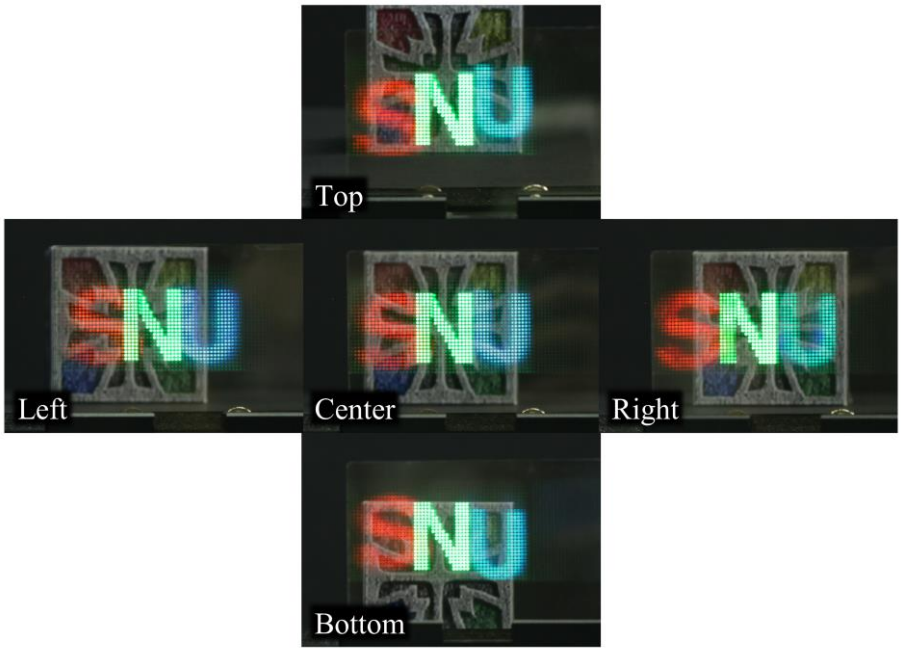

Figure 4.6 Perspective see-through 3D virtual images of three characters (‘S’, ‘N’, and ‘U’) with a real object ‘cube’ for a background, which are captured from five different view-positions in the displaying experiments.

Further work could investigate the use of a lens-array HOE which has a larger number of elemental lens HOEs with smaller lens pitch in order to reconstruct 3D virtual images with higher ray density to satisfy an accommodation depth cue [89, 90]. The real object ‘cube’ is also clearly observed along with the 3D virtual images through the full-color lens-array HOE, which verifies that the proposed AR system provides the see-through property. The experimental results support the validity of the full-color lens-array HOE for a novel scheme applicable to the autostereoscopic 3D display for the optical see-through AR system.

4.3 Viewing characteristic analysis on lens-array holographic optical elements

In this section, viewing characteristics for the lens-array HOE are discussed. Optical parameters for the recording scheme of the lens-array HOE and those for the lens-array itself are defined first, and then the viewing characteristics of reconstructed images on the lens-array HOE are presented in terms of these optical parameters. Additionally, novel frontal projection-type 2D/3D transparent screens are presented based on the analysis of the viewing characteristics for the lens-array HOE. Principles of 2D/3D imaging using a conventional lens-array are described, and the transparent screens which can provide 2D/3D imaging are implemented on the lens-array HOEs. The 2D/3D imaging conditions of the recorded lens-array HOEs are presented using the analyzed optical parameters. Lastly, feasibility of the proposed method is verified by the display experiments using the two lens-array HOEs with different optical parameters. The viewing characteristics of the proposed 2D/3D transparent screens are analyzed and also verified by the experiments.

4.3.1 Viewing characteristic of lens-array holographic optical elements

During the recording of a hologram, the optical properties of the reference lens-array are duplicated on the recorded lens-array HOE as a grating of interference patterns between the reference and signal waves. The viewing characteristics of displayed images on the lens-array HOE are closely related to the optical properties of the lens-array HOE. When the lens-array HOE is recorded by the scheme of reflection hologram as shown in Fig. 4.7(a), the optical properties of the lens-array HOE can be evaluated by the optical parameters depicted in Fig. 4.7(b). The lens-array HOE reconstructs the duplicated waves of the conventional lens-array with lens size p_{lens} and focal length f when a displaying beam corresponding to the reference wave in the hologram recording is projected from the image projector on the lens-array HOE. The size of the pixel on the projected image from the image projector is denoted by p_{proj}. The dimension of the projected pixel size is changed on the lens-array HOE because of the oblique projection angle (θ). The size of the projected pixel in the vertical direction is maintained as p_{proj}. In the horizontal direction, however, the pixel size is scaled to $p_{proj}/\cos\theta$ due to the oblique incidence on the horizontal plane. We denote the scaled pixel size in

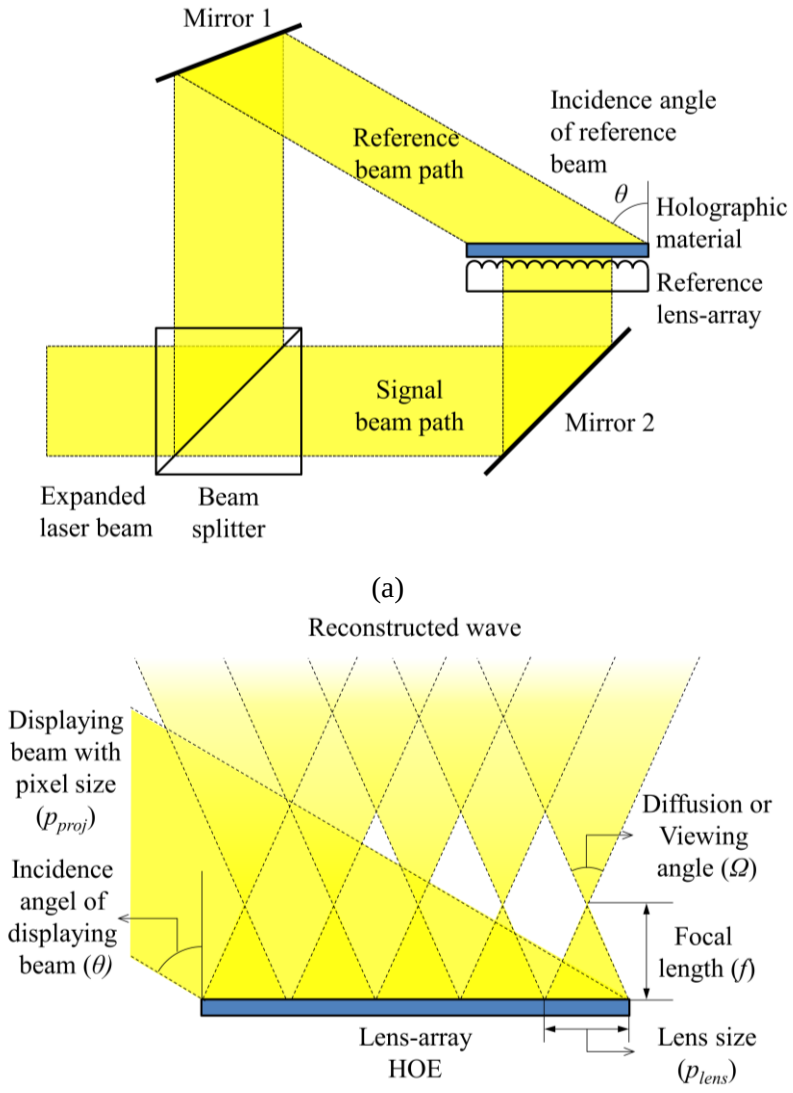

Figure 4.7 A schematic diagram of (a) recording the lens-array HOE by the reflection hologram scheme and (b) optical parameters of the recorded lens-array HOE.

the horizontal direction as p'_{proj}.

In the case of integral imaging, 3D images can be displayed within the limited viewing angle without any distortions. The viewing angle is one of the important viewing characteristics in integral imaging [88], and generally it depends on the specification of the elemental-lens. A diverging angle in the lens-array HOE corresponds to the viewing angle in the integral imaging. The diverging angle (Ω) of the lens-array HOE can be expressed by the optical parameters in Fig. 4.7(b) as

$$\Omega = 2\tan^{-1}\left(\frac{p_{lens}}{2f}\right). \tag{4.2}$$

A lateral resolution in the integral imaging is also an important viewing characteristic, and it is inversely proportional to the sizes of an elemental-lens. Therefore, the lateral resolution (R_l) of displayed autostereoscopic 3D images can be represented as

$$R_l = \frac{1}{p_{lens}} \tag{4.3}$$

Another important viewing characteristic of the 3D transparent screen is the angular resolution of the displayed 3D image [91]. The angular resolution in the integral imaging is defined by the number of perspectives per unit angle inside the viewing angle. Since each pixel behind the elemental-lens generates different perspectives, the number of perspectives in the case of

integral imaging is considered to be equal to that of pixels for the single elemental-lens. The angular resolution in the vertical direction (R_{av}) of the 3D transparent screen can be simply defined as

$$R_{av} = \frac{p_{lens}}{p_{proj}\Omega}. \tag{4.4}$$

On the other hand, the angular resolution in the horizontal direction (R_{ah}) is smaller than the angular resolution in the vertical direction due to the scaled projected pixel along the horizontal direction, and can be obtained as

$$R_{ah} = \frac{p_{lens}}{p'_{proj}\Omega}. \tag{4.5}$$

4.3.2 2D and 3D imaging on lens-array holographic optical elements with different viewing parameters

In this section, the 2D and 3D imaging conditions for the lens-array HOE are presented and the transparent 2D/3D screens are fabricated using these conditions. With the proper conditions are satisfied, the lens-array HOE can be used for transparent screen which can provide either 2D or 3D images on it [92-95]. Moreover, the viewing characteristics of the lens-array HOE are evaluated by comparing two lens-array HOEs recorded using two different

reference lens-arrays having different optical parameters.

The conventional lens-array has other applications to the autostereoscopic 3D imaging by the integral imaging, such as uniform illumination [92], distribution control of light [96-99], and 2D imaging screen [100]. Among them, the roles of the conventional lens-array as 2D/3D screens are discussed in this section. The function of the conventional lens-array as a 2D or 3D screen is determined by the relative size of an elemental-lens on the lens-array compared to the size of a projected pixel. Principles of 2D/3D imaging on the conventional lens-arrays are illustrated in Figs. 4.8 (a) and (b), respectively, when the elemental images are projected from the image projectors. In the figures, images are assumed to be projected in parallel to the optic-axis of the lens-array for the sake of simplicity, and the projected pixels, which have different colors and intensity information, are denoted as p_1, p_2, and p_3.

When the size of the elemental-lens is smaller than or equal to the size of the projected pixels, light from each pixel will diverge with a diffusing angle equivalent to the numerical aperture of the elemental-lens. In this case, the information on each pixel is maintained within the diffusing angle as the conventional diffuser, and 2D images are diffused in the observer's direction. Figure 4.8(a) shows 2D imaging on a lens-array when both the projected

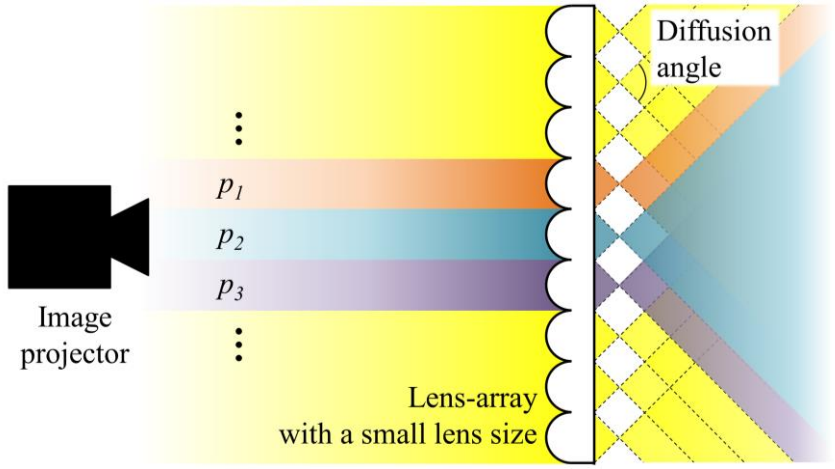

(a)

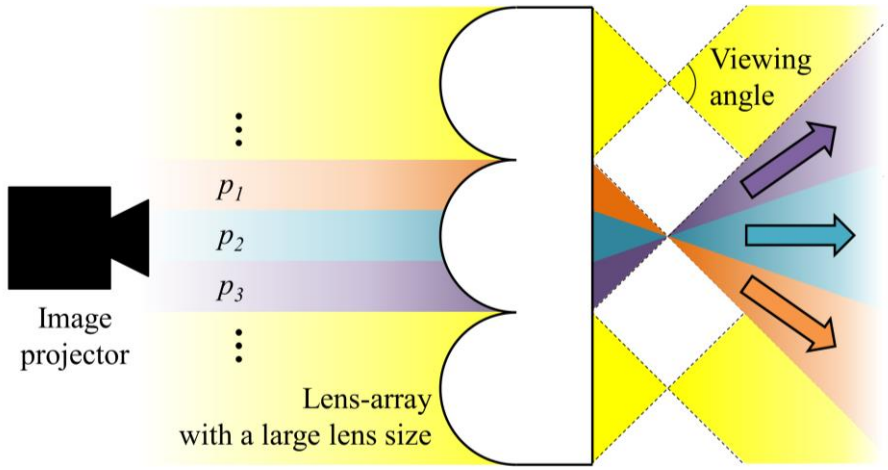

(b)

Figure 4.8 Principles of 2D/3D imaging on the conventional lens-array: (a) 2D imaging when the lens size is equal to or smaller than the projected pixel size, and (b) 3D imaging when the lens size is at least twice larger than the projected pixel size.

pixel and elemental-lens are the same size. On the other hand, 3D imaging can be achieved by a lens-array when the size of the elemental-lens is at least twice larger than the size of the projected pixel. When this condition is satisfied, every pixel projected on a one elemental-lens is crossed at the same focal point of the elemental-lens, and is then projected separately toward its refracted direction. This situation satisfies the principles of projection-type integral imaging, and the observer is able to observe full-parallax autostereoscopic 3D images within a viewing angle that is equivalent to the numerical aperture of the elemental-lens [101-103]. Figure 4.8(b) illustrates an example of 3D imaging on a lens-array when the size of the elemental-lens is three times larger than the sizes of the projected pixels.

This approach of describing the 2D and 3D imagings on the conventional lens-array can be also applied to the lens-array HOE. By simply varying the optical parameters of the lens-array HOE, it can be used as transparent 2D and 3D screens. The dimensional features of the proposed transparent screens based on the lens-array HOEs are determined by the relation between p_{lens} and p'_{proj} as follows:

$$p_{lens} < p'_{proj} \quad \text{for 2D transparent screen,} \tag{4.6}$$

$$p_{lens} \geq 2p'_{proj} \quad \text{for 3D transparent screen.} \tag{4.7}$$

The optical parameters, p_{lens} and f, are to be decided by the specifications of the reference lens-array, and p_{proj} can be adjusted by the image projector. Therefore, the 2D and 3D features of the proposed transparent screens can be implemented by choosing the appropriate reference lens-arrays and image projectors according to the conditions given in Eqs. (4.6) and (4.7).

The transparent property of the proposed 2D and 3D screens is achieved by the principles of a volume hologram. The lens-array HOE functions as a 2D or 3D screen only for Bragg matched incident light with the wavelength and incidence angle that are identical to those of the reference beam used in recording the hologram [25, 26]. For other light from the real world scene, except for the Bragg matched light, the lens-array HOE has no effect on any optical functions because the light simply passes through it as if it were a transparent film.

4.3.3 Experiments

Two lens-array HOEs are recorded by using the two different reference lens-arrays commercially available in Refs. [104, 105]. The specifications of the reference lens-arrays for the 2D/3D transparent screens are listed in Table 4.2. The size of the lens in the reference lens-array for the 3D transparent screen

is relatively larger, 1 mm, with a focal length of 3.3 mm, compared to that for the 2D transparent screen which has a lens size of 0.125 mm and a focal length of 0.4 mm. The diffusion and viewing angles of the recorded lens-array HOEs calculated by Eq. (4.2), are 17.8° and 17.2°, respectively. The size of the recorded lens is also related to the lateral resolutions of the 2D/3D transparent screens as discussed in the previous section. The lateral resolutions for the 2D and 3D transparent screens are 8 pixels/mm and 1 pixels/mm, respectively. In this experimental setup, both 2D and 3D transparent screens are recorded in the shape of a circle with a diameter of 45 mm.

Diffraction efficiencies for red, green, and blue colors on the recorded lens-array HOEs are directly related to the color representation in the display procedure. In order to display appropriate colors on the proposed transparent screens, the diffraction efficiencies for the three colors must be carefully adjusted by controlling exposure energies during the recording of both lens-array HOEs for the 2D/3D transparent screens. Exposure conditions and measured diffraction efficiencies for both 2D and 3D transparent screens are listed in Table 4.3. A spectrometer (Ocean Optics, USB4000-VIS-NIR) with a white light source (Ocean Optics, HL-2000-FHSA) is used for measuring diffraction efficiencies of both lens-array HOEs [94]. As shown in Table 4.3,

Table 4.2 Conventional lens-arrays that are used as reference lens-arrays to record the lens-array HOEs for 2D/3D transparent screens

	For 2D screen	For 3D screen
Commercial Model	Grapac HALS-PP400	Fresneltech 630
Lens size (p_{lens})	0.125 mm	1 mm
Focal length (f)	0.4 mm	3.3 mm
Diffusion or viewing angle (Ω)	17.8˚	17.2˚

Table 4.3 Exposed energies and diffraction efficiencies for red, green, and blue colors on the implemented 2D/3D transparent screens

		2D screen	3D screen
Exposed energy (mJ/cm^2)	Red	20.5	28.7
	Green	39.4	34.9
	Blue	47.4	51.1
Diffraction efficiency (%)	Red	19.7	19.1
	Green	20.3	23.2
	Blue	24.3	22.1

both lens-array HOEs provided similar values of diffraction efficiencies for red, green, and blue colors: 19.7 %, 20.3 %, and 24.3 % on the 2D transparent screen, and 19.1 %, 23.2 %, and 22.1 % on the 3D transparent screen, respectively. Photographs of the recorded lens-array HOEs for 2D/3D transparent screens under white light are shown in Figs. 4.9(a) and 4.9(b), respectively.

Since the reference lens-array used for recording the 2D transparent screen has a low fill factor with a 180 μm lens pitch and a 125 μm lens size, it partially performs the function of a diffusor and an undesirable function of a mirror at the same time. This ambiguous problem, however, can be simply solved by using a reference lens-array with a high fill factor in the recording procedure. The diffusion angle of the lens-array HOE for the 2D transparent screen is evaluated using the measurement setup shown in Fig. 4.10(a). A collimated laser beam with a beam waist of 5 mm and a wavelength of 532 nm is incident on the HOE with incidence angle θ, which is identical to that in the recording setup. The diameter of the area of diffused light superimposed on purely reflected light is 41 mm, and it is measured at a distance of 120 mm from the HOE, as seen in Fig. 4.10(b). From these measured values, the diffusion angle for the 2D transparent screen is 17.1° which approximates to the calculated value in Table 4.2.

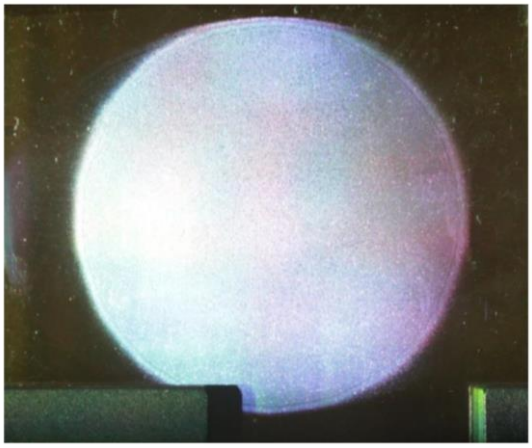

(a)

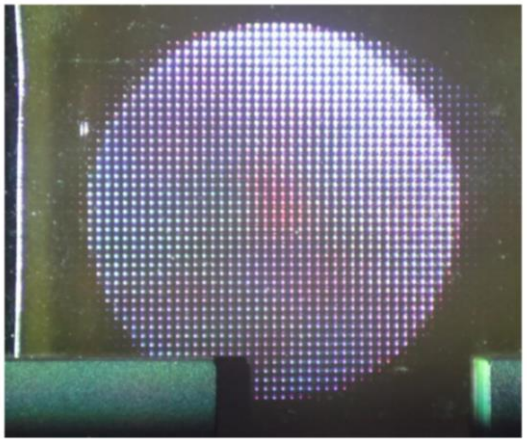

(b)

Figure 4.9 Recorded lens-array HOEs for (a) 2D and (b) 3D transparent screens.

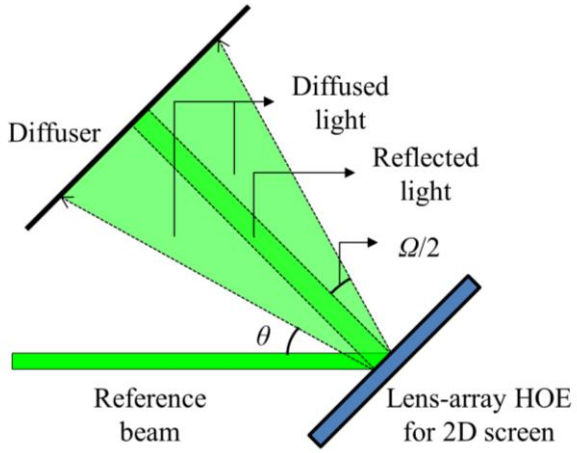

(a)

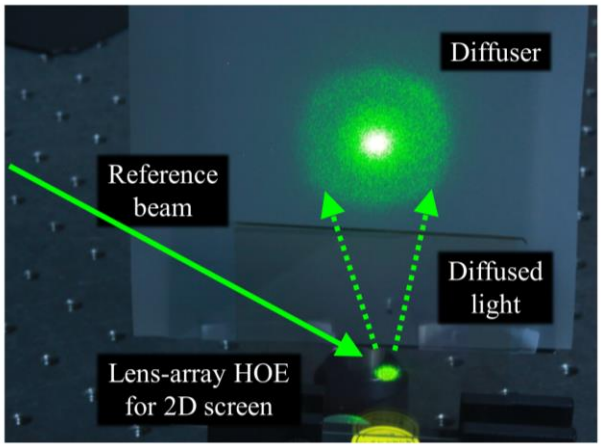

(b)

Figure 4.10 Measurement of the diffusion angle Ω on the lens-array HOE for the 2D transparent screen: (a) a schematic diagram of optical paths of light, and (b) a photograph of the measurement setup.

In order to demonstrate the proposed transparent screens, display experiments is carried out by using the lens-array HOEs and an image projector. The lens-array HOE as a proposed transparent screen is located on the path of the image projection with an incident angle of 45˚, which is identical to that of the reference beam path in the hologram recording setup. A background object ‘cube’ is located behind the transparent screen to confirm the transparent property of our proposed method. The sizes of the projected pixels (p_{proj}) are adjusted by relay optics and the telecentric lens to be 128 μm and 25.6 μm for the 2D/3D transparent screens, respectively. These sizes of projected pixels are slightly larger and about 40 times smaller than the size of elemental-lenses on lens-array HOEs used for the 2D and 3D transparent screens, respectively, which satisfy the 2D/3D imaging conditions. The angular resolutions, calculated by Eqs. (4.4) and (4.5) are 1.6 perspectives/degree and 2.3 perspectives/degree in the horizontal and vertical directions of the 3D transparent screen, respectively.

When the 2D images shown in Fig. 4.11(a) are projected from the image projector, the see-through 2D images are captured on the proposed 2D transparent screen, as seen in Fig. 4.11(b) with the background object appearing behind the transparent screen. Since the proposed 3D transparent screen provides 3D images based on the principles of the projection-type

integral imaging, the elemental images must be projected [101-103]. The elemental images used in the display experiment for the 3D transparent screen are generated by computer graphics. They include 3D information related to the three characters ‘O’, ‘S’, and ‘A’ of red, green, and blue colors with a depth discrepancy of 20 mm, 0 mm, and -20 mm, respectively. From the elemental images shown in Fig. 4.12(a), the 3D images are produced around the 3D transparent screen with the background scene of the real object ‘cube’, as shown in Fig. 4.12(b), captured from five different viewing directions. The top/right and bottom/left perspective images are captured 8˚ and -8˚ apart from the viewing position of the center perspective image, respectively. From these captured positions, the viewing angle for the 3D transparent screen is 16˚. The feasibility of the proposed 2D/3D transparent screens is clearly verified from the results of the display experiments. In the case of the 2D transparent screen, the projected 2D images are properly diffused on the 2D transparent screen with their colors maintained. The 3D imaging on the proposed 3D transparent screen is also verified by the appropriate disparities among the three virtual characters from five different viewing directions. In both cases, the background object can clearly be observed through the transparent screens, which confirms the transparent property of the proposed 2D/3D screens.

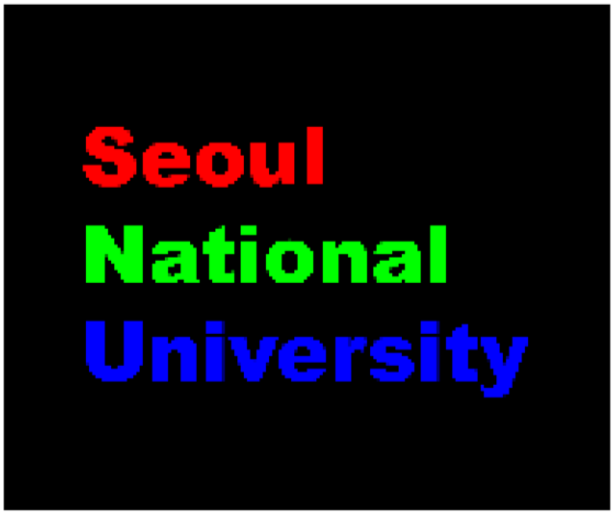

(a)

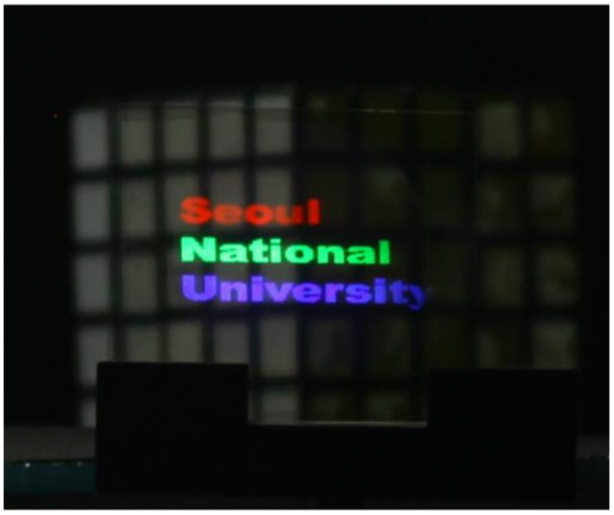

(b)

Figure 4.11 Images for the 2D transparent HOE screen: (a) 2D images projected to the screen, and (b) see-through 2D images displayed on the screen with a real object ‘cube’ for a background.

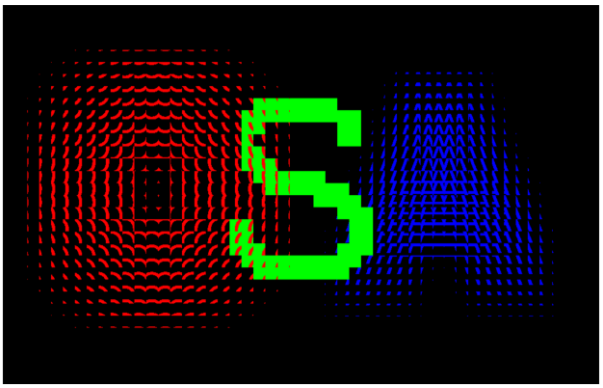

(a)

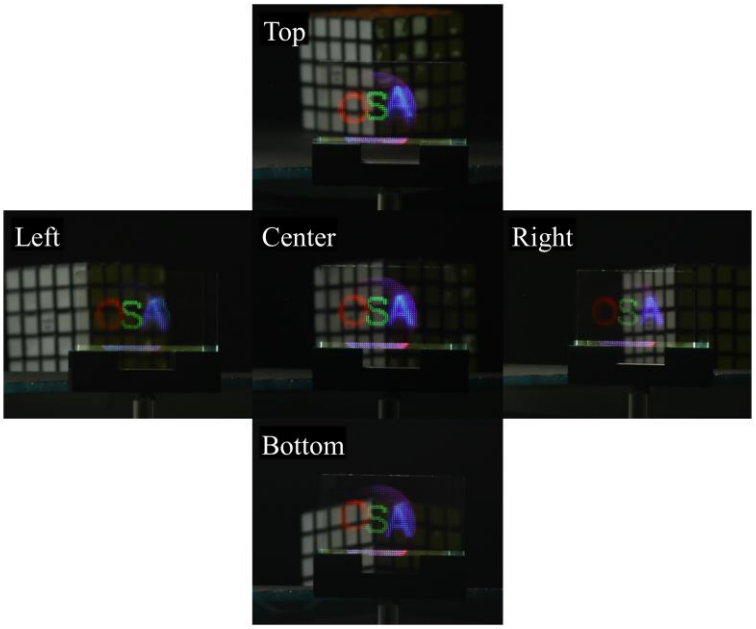

(b)

Figure 4.12 Images for the 3D transparent HOE screen: (a) elemental images projected to the screen, and (b) perspective see-through 3D images around the screen captured from five different viewing directions with a background object ‘cube’.

Regarding further possibilities for the proposed method, we note that it is also possible to simultaneously display both 2D and 3D virtual images on the proposed lens-array HOE. In the recording procedure, two lens-arrays satisfying the 2D/3D imaging conditions presented in Eqs. (4.6) and (4.7) respectively, can be recorded on the same area of the photopolymer by an angular multiplexing technique by using two reference beams with different incident angles. Then, the two image projectors, which satisfy both the 2D/3D imaging conditions and incident angles, can display both 2D and 3D contents at the same time in the angular multiplexed lens-arrays HOE. Since the photopolymer has a limited dynamic range, however, we give a higher priority to the wavelength multiplexing for full-color imaging than the other multiplexing techniques. Hence, the production of 2D and 3D transparent screens is separately realized on different types of lens-array HOEs. If a photopolymer with a higher dynamic range are available, however, both 2D and 3D transparent screens could be recorded together on the same area of the photopolymer by using an angular multiplexing technique. It would then be possible to simultaneously display full-color 2D and 3D images on a single transparent screen by two image projectors which have different projection angles.

4.4 Dynamic autostereoscopic 3D images displayed on the lens-array HOE

Different from the holographic stereogram which merges the functionalities of the SLM and optical layer for the autostereoscopic 3D display into a layer of the static hologram, the autostereoscopic 3D display using the lens-array HOE has an external SLM for providing intensity modulated images onto the lens-array HOE. Therefore, the autostereoscopic 3D display using the lens-array HOE can provide dynamic 3D images to the viewers. In this section, experiments for displaying dynamic images on the lens-array HOE are performed. The dynamic elemental images are generated by computer graphics. In the first frame of the dynamic elemental images, two moving objects located on the *z*-axis, 'magenta square' and 'yellow diamond', have depth information of 15 mm and -15 mm, respectively. In each frame of the dynamic elemental images, both objects are making a 1˚ of rotation around the *y*- and *x*-axis. Totally 360 single elemental images are computationally captured for generating the dynamic elemental images. Figure 4.13 shows the selected single-frame excerpts from the generated dynamic elemental images. The dynamic elemental images are displayed on the lens-array HOE using the displaying experimental setup shown in Fig. 4.5(a).

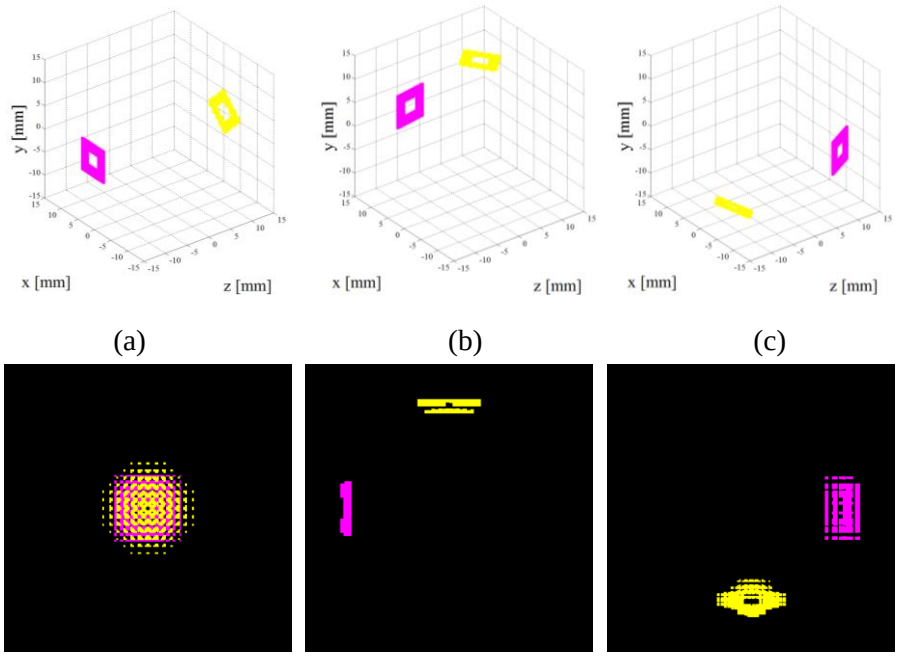

Figure 4.13 Selected single-frame excerpts from the dynamic elemental images: (a), (b), (c) positions of object ‘square’ and ‘diamond’, and (d), (e), (f) excerpted elemental images from 1st , 80th, and 240th frame, respectively.

Figure 4.14 shows the resultant dynamic autostereoscopic 3D images captured at the 1^{st} , 80^{th} , and 240^{th} frames of the dynamic elemental images, respectively. It is clearly confirmed that the autostereoscopic 3D display using the lens-array HOE can properly provide dynamic autostereoscopic 3D images.

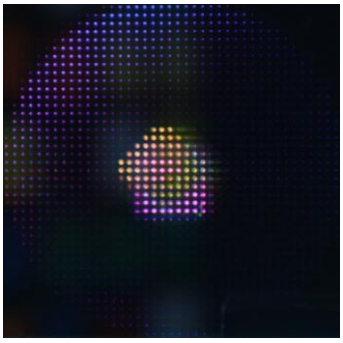

(a)

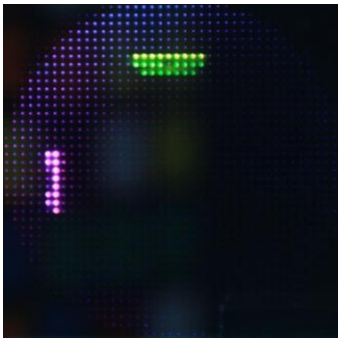

(b)

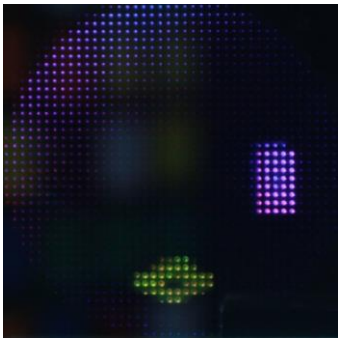

(c)

Figure 4.14 Captured dynamic 3D images displayed by the autostereoscopic 3D display using the lens-array HOE: captured at 1st , 80th , and 240th frame of the dynamic elemental images, respectively.

4.5 Results

The lens-array HOE for displaying the autostereoscopic 3D images is proposed. The lens-array HOE is fabricated on the photopolymer by the reflection hologram recording technique to gain advantages of see-through property, thin thickness, and low cost which are unobtainable from conventional methods for the autostereoscopic displays. The proposed full-color lens-array HOE is applicable especially to the 3D optical see-through AR systems in virtue of its see-through property. The HOE recording setup is built for fabricating the lens-array HOE. The recording setup can apply the wavelength multiplexing and spatial multiplexing for the full-color imaging and large-area recording, respectively. Experimental results for displaying the autostereoscopic 3D virtual images in the proposed system reveal the feasibility of the 3D imaging with see-through and full-color properties which are essential conditions for the 3D optical see-through AR system.

Furthermore, viewing characteristics, such as the viewing angle, lateral resolution, and angular resolution, for the displayed 3D images on the proposed method are evaluated by the optical parameters of the lens-array HOEs. Based on the analysis of the viewing characteristics, possibilities of the lens-array HOEs for the applications of 2D and 3D transparent screens

are discussed. Two lens-array HOEs with different specifications are made for 2D/3D transparent screens. The elemental-lens and projected pixel of the recorded lens-array HOE for a 2D transparent screen are almost the same sizes. On the other hand, the lens-array HOE for a 3D transparent screen has an elemental-lens that is 40 times larger than the projected pixel size. Experimental results for displaying 2D/3D images on the proposed 2D/3D transparent screens verify the validity of 2D/3D imaging by the lens-array HOEs, in which the see-through property is satisfactory. We expect that the proposed see-through 2D and 3D imaging methods on the lens-array HOE with the possibility of simultaneous 2D and 3D imaging have the potential for use in a wide variety of applications in virtual reality systems.

Chapter 5 Conclusion and recommendation for future work

5.1 Conclusion

The autostereoscopic 3D display implemented by adopting the holographic recording techniques has been investigated in this dissertation research. The main purpose of the research is the development of novel methods for displaying high resolution and see-through autostereoscopic 3D images which cannot be provided by conventional autostereoscopic 3D display methods due to their limitations.

The optical characteristics of the photopolymer film are numerically and experimentally analyzed to evaluate its suitability for the use as a holographic material for the imaging purpose. The optical properties of the photopolymer are evaluated at three different wavelengths of 671 nm, 532 nm, and 473 nm, which correspond to the three primary colors of red, green, and blue, respectively. Nearly 100 % of saturated diffraction efficiencies for

the three wavelengths are revealed by the experiments of measuring dosage responses at the three single-wavelength hologram recordings. A wavelength multiplexed hologram is recorded using the three lasers which have wavelengths of the primary colors. With the proper recording conditions, almost the same diffraction efficiencies of around 50 % are measured at the three primary colors from the three-wavelength multiplexed hologram. These measured similar diffraction efficiencies satisfy the wavelength multiplexing property of the photopolymer film which is an essential requirement to the full-color recording and imaging. The shrinkage of the photopolymer film during the recording procedure is theoretically analyzed, and it shows that the shrinkages along the length and thickness directions affect the direction of reconstructed beam and the diffraction efficiency, respectively. The measured values of the shrinkage rate changes for the photopolymer along the length and thickness directions are 0 % and 2.6 %, respectively.

As the first suggestion of the holographic recording technique, a hogel overlapping method is presented for generating high resolution holographic stereograms. By using the holographic printing method, the SLM and the optical layer in the conventional autostereoscopic 3D display can be merged into a single hologram recorded in the photopolymer film. However, the enhancement of the lateral resolution of the holographic stereogram is

limited because high frequency components of the image information are lost during the holographic printing procedure when the size of recorded hogel decreases. The lateral resolution can be enhanced by the hogel printing in the overlapped region. This resolution enhancement from the hogel overlapping method is accomplished by taking advantage of multiplexing property of the volume hologram recorded in the photopolymer film. The holographic printing system which can perform the hogel overlapping method is built. The two holographic stereograms are optically recorded by using the conventional and hogel overlapping holographic recording methods. The holographic stereogram generated by the hogel overlapping method has a lateral resolution enhanced by 4 times compared to the conventional method. Although the lateral resolution is enhanced by 4 times in the experiment, this value can be enhanced more than factor of 4 if the photopolymer film has a higher dynamic range. Comparison of the two holographic stereograms verifies the feasibility of the lateral resolution enhancement of the holographic stereogram by the hogel overlapping method.

Another holographic recording technique suggested in this dissertation is a hologram recording method for fabricating the lens-array HOEs. The optical function of the lens-array HOE is identical to those of the conventional lens-array, which is the optical layer used in the integral

imaging. The HOE recording setup is built for fabricating the lens-array HOE, and it can apply the wavelength multiplexing and spatial multiplexing for the full-color imaging and large-area recording, respectively. By using this holographic recording setup, a 30 mm × 60 mm sized full-color lens-array HOE having 1 mm lens pitch has been fabricated. The fabricated full-color lens-array HOE has similar diffraction efficiencies of around 20 % at the three primary colors. Experimental results for displaying the autostereoscopic 3D virtual images on the lens-array HOE reveal the feasibility of its full-color 3D imaging and see-through properties. The limitations on the conventional lens-array are improved by replacing it with the lens-array HOE, because the lens-array HOE is fabricated by the optical recording process on the photopolymer in a thin structure. Furthermore, the lens-array HOE is applicable especially to the 3D optical see-through AR systems in virtue of its see-through property.

In addition, the viewing characteristics, such as viewing angle, lateral resolution, and angular resolution, for the displayed autostereoscopic 3D images on the proposed method are evaluated by optical parameters of the lens-array HOEs. Two lens-array HOEs with different optical parameters are fabricated. One has almost the same sizes of elemental-lens to the pitch of the projected pixel, and another one has the elemental-lens size 40 times

larger than the pitch of the projected pixel. With these two fabricated lens-array HOEs, the possibility of the use of the lens-array HOEs as the 2D and 3D transparent screens is discussed, and experimental results of 2D and 3D imaging on the lens-array HOEs are presented. Experimental results for displaying 2D/3D images on the lens-array HOEs prove the validity of the lens-array HOEs for the 2D/3D imaging with satisfactory see-through property.

5.2 Recommendation for future work

Although the limitations of conventional autostereoscopic 3D display can be improved by the holographic recording techniques presented in this dissertation, further studies are recommended to display more realistic 3D virtual images by using the presented work.

The first recommendation for further research is to integrate the holographic recording techniques presented in this dissertation: holographic printing (Chapter 3) and HOE recording (Chapter 4). This can be done by a sequential HOE recording by the holographic printing technique. One limitation on the holographic recording technique for fabricating lens-array HOEs in this dissertation is the difficulty in adjusting optical parameters of the lens-array HOE because the lens-array HOE can have only the same optical characteristics as the reference lens-array. However, the recommended idea makes it possible to implement a customizable lens-array HOE. Figure 5.1 shows a schematic diagram of the concept of the sequential recording of elemental-lens HOEs by adopting the holographic printing technique. Unlike the holographic printer, which uses an SLM to record perspective information on the hogels, the presented method does not use an SLM in the recording procedure. Instead of recording hogel, this method

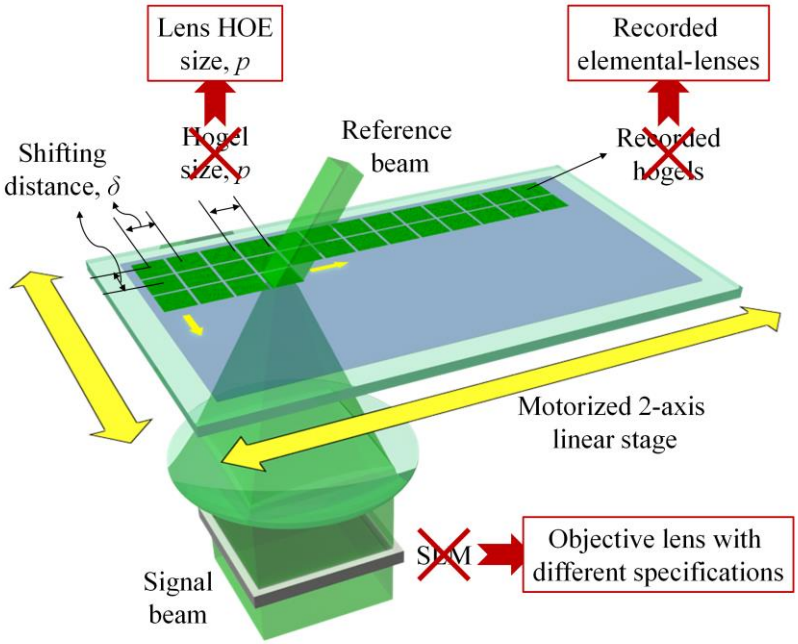

Figure 5.1 A schematic diagram of the sequential recording of elemental-lens HOEs for a customized lens-array HOE by adopting the holographic printing method.

records the optical properties of the objective lens in the signal beam path into the photopolymer as an elemental-lens HOE. After the sequential recording of these elemental-lens HOEs along the vertical and horizontal directions, a lens-array HOE can be fabricated by the presented method. The strength of the recommended method is the capability of customizing the optical parameters of fabricated lens-array HOEs. The optical characteristics of the elemental-lens HOEs are determined by specifications of the objective lens used in the recording procedure. Therefore, the lens-array HOE fabricated by the recommended holographic recording technique can have customized optical characteristics.

The second recommendation for further work is to implement an optical layer which has an arbitrary surface. Although all the holograms fabricated in this dissertation are recorded on the flat plane, both holographic stereogram and HOEs can be recorded on arbitrary surfaces by virtue of flexible characteristics of the photopolymer film. However, hologram recording on a non-flat surface introduces a lot of difficulties, such as numerical analysis of hologram formation, configurations of experimental setup for hologram recording, analysis of shrinkage, and so on. If the autostereoscopic 3D display can be implemented on arbitrary surfaces, it is expected that the applications of this technique will be widely spread to holographic recording

and display markets.

Lastly, an appropriate color representation is one of the issues on the autostereoscopic 3D display implemented by using holographic recording techniques. Since most of holographic materials, including photopolymer film, have a nonlinear dosage response characteristic, it is hard to reproduce intended colors in the display procedure. Therefore, a clear understanding of the nonlinear dosage response of holographic material in the recording procedure, and a color correction or compensation method in the display procedure are required.

Bibliography

1. T. Okoshi, “Three-dimensional displays,” in Proc. IEEE **68**, 548-564 (1980).
2. J. Hong, Y. Kim, H.-J. Choi, J. Hahn, J.-H. Park, H. Kim, S.-W. Min, N. Chen, and B. Lee, “Three-dimensional display technologies of recent interest: principles, status, and issues,” Appl. Opt. **50**, H87-H115 (2011).
3. J. Geng, “Three-dimensional display technologies,” Adv. Opt. Photon. **5**, 456-535 (2013).
4. B. Lee, “Three-dimensional displays, past and present,” Physics Today, **66**, 36-41 (2013).
5. B. Lee, “3D display - where we are and where to go,” in Biomedical Optics, OSA Technical Digest (Optical Society of America, 2012), paper JM1A.2.
6. I. Sexton and Y. Surman, “Stereoscopic and autostereoscopic display systems,” Signal Process. Mag. **16**, 85–99 (1999).
7. S. Nagata, “How to reinforce perception of depth in single two-dimensional pictures,” Proc. SID **25**, 239-246 (1984).
8. G. R. Jones, D. Lee, N. S. Holliman, and D. Ezra, “Controlling perceived depth in stereoscopic images,” Proc. SPIE **4297**, 42 (2001).

9. B. A. Wandell, *Foundations of Vision* (Sinauer Associates, 1995).
10. B. A. Steinman, and R. P. Garzia, *Foundations of Binocular Vision: a Clinical Perspective* (McGraw-Hill, 2000).
11. S. S. Kim, B. H. You, H. Choi, B. H. Berkeley, D. G. Kim, and N. D. Kim, "World's first 240Hz TFT-LCD technology for full-HD LCD-TV and its application to 3D display" in Proc. SID **40**, 424–427 (2009).
12. D.-S. Kim, S.-M. Park, J.-H. Jung, and D.-C. Hwang, "New 240Hz driving method for full HD and high quality 3D LCD TV," in Proc. SID **41**, 762–765 (2010).
13. H. Kang, S.-D. Roh, I.-S. Baik, H.-J. Jung, W.-N. Jeong, J.-K. Shin, and I.-J. Chung, "A novel polarizer glasses-type 3D displays with a patterned retarder," in Proc. SID **41**, 1–4 (2010).
14. B. Mendiburu, *3D TV and 3D Cinema: Tools and Processes for Creative Stereoscopy* (Taylor & Francis, 2011).
15. J. Wann, S. Rushton, and M. Mon-Williams, "Natural problems in the perception of virtual environments," Vision Res. **35**, 2731–2736 (1995).
16. T. Inoue and H. Ohzu, "Accommodation responses to stereoscopic three-dimensional display," Appl. Opt. **36**, 4509–4515 (1997).
17. F. L. Kooi and A. Toet, "Visual comfort of binocular and 3D displays," Displays **25**, 99–108 (2004).

18. M. Lambooij, W. IJsselsteijn, M. Fortuin, and I. Heynderickx, “Visual discomfort and visual fatigue of stereoscopic displays: a review,” J. Imaging Sci. Technol. **53**, 030201 (2009).
19. N. A. Dodgson, “Autostereoscopic 3D displays,” Computer **38**, 31–36 (2005).
20. A. Kubota, A. Smolic, M. Magnor, M. Tanimoto, T. Chen, and C. Zhang, “Multiview imaging and 3DTV,” IEEE Signal Process. Mag. **24**, 10–21 (2007).
21. Ultimate Holography. http://www.ultimate-holography.com
22. D. H. Close, “Holographic optical elements,” Opt. Eng. **14**, 408 (1975).
23. I. Kasai, Y. Tanijiri, T. Endo, and H. Ueda, “A practical see-through head mounted display using a holographic optical element,” Opt. Rev. **8**, 241–244 (2001).
24. P. Hariharan, *Basics of Holography* (Cambridge University Press, 2002).
25. R. R. A. Syms, *Practical Volume Holography* (Oxford: Clarendon Press, 1990).
26. K. Curtis, L. Dhar, A. Hill, W. Wilson, and M. Ayres, *Holographic Data Storage* (Wiley, 2010).
27. G. K. Ackermann, and J. Eichler, *Holography: A Practical Approach* (John Wiley & Sons, 2007).

28. F.-K. Bruder, R. Hagen, T. Rölle, M.-S. Weiser, and T. Fäcke, “From the surface to volume: concepts for the next generation of optical-holographic data-storage materials,” Angew. Chem. Int. Ed. **50**, 4552–4573 (2011).
29. R. Kurtz and R. Owen, “Holographic recording materials—A review,” Opt. Eng. **14**, 393 (1975).
30. P. Hariharan, “Holographic recording materials: Recent developments,” Opt. Eng. **19**, 636 (1980).
31. G. Saxby, *Practical Holography* (Prentice-Hall, 1988).
32. W. Colburn and K. Haines, “Volume hologram formation in photopolymer materials,” Appl. Opt. **10**, 1636-1641 (1971).
33. E. S. Kim and N. Kim. “Press-based colour tuning process to control playback wavelength of holograms.” Elec. Lett. **39**, 1846-1847 (2003).
34. K. Lee, S. Jeung, B. Cho, and N. Kim, “Photopolymer-based surface-normal input/output volume holographic grating coupler for 1550-nm optical wavelength,” J. Opt. Soc. Korea **16**, 17-21 (2012).
35. J. Piao, G. Li, M. Piao, and N. Kim, “Full color holographic optical element fabrication for waveguide-type head mounted display using photopolymer,” J. Opt. Soc. Korea **17**, 242-248 (2013).
36. M. Piao and N. Kim, “Achieving high levels of color uniformity and

optical efficiency for a wedge-shaped waveguide head-mounted display using a photopolymer," Appl. Opt. **53**, 2180-2186 (2014).

37. A. Pu and D. Psaltis, "High-density recording in photopolymer-based holographic three-dimensional disks," Appl. Opt. **35**, 2389-2398 (1996).
38. A. Pu, K. Curtis, and D. Psaltis, "Exposure schedule for multiplexing holograms in photopolymer films," Opt. Eng. **35**, 2824–2829 (1996).
39. R. Kostuk, "Dynamic hologram recording characteristics in DuPont photopolymers," Appl. Opt. **38**, 1357-1363 (1999).
40. P. Wu, Z. Liu, J. Yang, A. Flores, and M. Wang, "Wavelength-multiplexed submicron holograms for disk-compatible data storage," Opt. Express **15**, 17798-17804 (2007).
41. A. Bloom, R. A. Bartolini, and D. L. Ross, "Organic recording medium for volume phase holography," Appl. Phys. Lett. **24**, 612 (1974).
42. G. Zhao and P. Mouroulis, "Diffusion model of hologram for-mation in dry photopolymer materials," J. Mod. Opt. **41**, 1929–1939 (1994).
43. M. Gleeson and J. Sheridan, "Nonlocal photopolymerization kinetics including multiple termination mechanisms and dark reactions. part I. modeling," J. Opt. Soc. Am. B **26**, 1736-1745 (2009).
44. M. Gleeson, S. Liu, R. McLeod, and J. Sheridan, "Nonlocal photopolymerization kinetics including multiple termination mechanisms

and dark reactions. part II. experimental validation," J. Opt. Soc. Am. B **26**, 1746-1754 (2009).

45. M. Gleeson, S. Liu, J. Guo, and J. Sheridan, "Non-local photo-polymerization kinetics including multiple termination mechanisms and dark reactions: part III. primary radical generation and inhibition," J. Opt. Soc. Am. B **27**, 1804-1812 (2010).
46. M. Gleeson, J. Sheridan, F. Bruder, T. Rolle, H. Berneth, M. Weiser, and T. Facke, "Comparison of a new self developing photopolymer with AA/PVA based photopolymer utilizing the NPDD model," Opt. Express **19**, 26325-26342 (2011).
47. G. Wyszecki and W. Stiles, *Color Science: Concepts and Methods, Quantitative Data and Formulae*, 2nd ed. (Wiley, 1982).
48. G. W. Meyer, "Tutorial on color science", Visual Computer **2**, 278 -290 (1986).
49. E. Buckley, "Laser wavelength choices for pico-projector applications," J. Disp. Technol. **7**, 402–406 (2011).
50. I. Wallhead, R. Ocaña, and P. Quinzá, "Designing a laser scanning picoprojector. part 1. characteristics of the optical displaying system and color-management-related issues," Appl. Opt. **51**, 4803 (2012).
51. M.-L. Hsieh and K. Y. Hsu, "Grating detuning effect on holographic

memory in photopolymers,” Opt. Eng. **40**, 2125-2133 (2001).

52. L. Dhar, M. G. Schnoes, T. L. Wysocki, H. Bair, M. Schilling, and C. Boyd, ‘‘Temperature-induced changes in photopolymer volume holograms,’’ Appl. Phys. Lett. **73**, 1337–1339 (1998).
53. M. G. Schnoes, L. Dhar, M. L. Schilling, S. S. Patel, and P. Wiltzius, “Photopolymer-filled nanoporous glass as a dimensionally stable holographic recording medium,’’ Opt. Lett. **24**, 658–660 (1999).
54. M. Moothanchery, I. Naydenova, and V. Toal, “Study of the shrinkage caused by holographic grating formation in acrylamide based photopolymer film,” Opt. Express **19**, 13395-13404 (2011).
55. H. Kogelnik, “Coupled wave theory for thick hologram gratings,” Bell Syst. Tech. J. 48, 2909–2947 (1969).
56. S. A. Benton, “Survey of holographic stereograms,” Proc. SPIE **367**, 15 (1982).
57. M. Lucente, “Diffraction-specific fringe computation for electro-holography,” Ph. D. Thesis, Department of Electrical Engineering and Computer Science, Massachusetts Institute of Technology (1994).
58. S. J. Daly, R. T. Held, and D. M. Hoffman, “Perceptual issues in stereoscopic signal processing,” IEEE Trans. Broadcast **57**, 347-361 (2011).

59. Y. H. Kang, K. H. Kim, and B. Lee, “Volume hologram scheme using optical fiber for spatial multiplexing,” Opt. Lett. **22**, 739-741 (1997).

60. Y. H. Kang, K. H. Kim, and B. Lee, “Angular and speckle multiplexing of photorefractive holograms by use of fiber speckle patterns,” Appl. Opt. **37**, 6969–6972 (1998).

61. M. Yamaguchi, N. Ohyama, and T. Honda, “Holographic 3-D printer,” in Proc. SPIE **1212**, 84-92 (1990).

62. M. Yamagucchi, H. Sugiura, T. Honda, and N. Ohyama, “Automatic recording method for holographic three-dimensional animation,” J. Opt. Soc. Am. A. **9**, 1200-1205 (1992).

63. M. Yamaguchi, T. Koyama, H. Endoh, and N. Ohyama, “Development of a prototype full-parallax holoprinter,” Proc. SPIE **2406**, 50 (1995).

64. M. Yamaguchi, N. Ohyama, and T. Honda, “Holographic three-dimensional printer: new method,” Appl. Opt. **31**, 217-222 (1992).

65. N. Peyghambarian, S. Tay, P.-A. Blanche, R. Norwood, and M. Yamamoto, “Rewritable holographic 3D displays,” Opt. Photon. News **19**, 22-27 (2008).

66. S. Tay, P.-A. Blanche, R. Voorakaranam, A. V. Tunc, W. Lin, S. Rokutanda, T. Gu, D. Flores, P. Wang, G. Li, P. St Hilaire, J. Thomas, R. A. Norwood, M. Yamamoto, and N. Peyghambarian, “An updatable

holographic three-dimensional display," Nature **451**, 694-698 (2008).

67. P.-A. Blanche, A. Bablumian, R. Voorakaranam, C. Christenson, W. Lin, T. Gu, D. Flores, P. Wang, W.-Y. Hsieh, M. Kathaperumal, B. Rachwal, O. Siddiqui, J. Thomas, R. A. Norwood, M. Yamamoto, and N. Peyghambarian, "Holographic three-dimensional telepresence using large-area photorefractive polymer," Nature **468**, 80-83 (2010).
68. M. Klug, M. Holzbach, and A. Ferdman, "Method and apparatus for recording 1-step full-color full-parallax holographic stereograms," U.S. Patent No. US6330088B1 (1998).
69. M. Klug, M.E. Holzbach, and A. J. Ferdman, "Apparatus and method for replicating a hologram using a steerable beam," U.S. Patent No. US6266167B1 (2001).
70. D. Brotherton-Ratcliffe, F. M. Vergnes, A. Rodin, and M. Grichine, "Holographic Printer," U.S. Patent No. US7800803B2 (1999).
71. A. Rodin, F. M. Vergnes, and D. Brotherton-Ratcliffe, "Pulsed multiple colour laser," EU Patent No, EPO 1236073 (2001).
72. D. Brotherton-Ratcliffe, S. J. Zacharovas, R. J. Bakanas, J. Pileckas, A. Nikoskij, and J. Kuchin, "Digital holographic printing using pulsed RGB lasers," Opt. Eng. **50**, 091307 (2011).
73. J. Goodman, *Introduction to Fourier Optics* (McGraw-Hill, 1968).

74. F. H. Mok, G. W. Burr, and D. Psaltis, “A system metric for holographic memory systems,” Opt. Lett. **21**, 896–898 (1996).

75. D. W. F. van Krevelen and R. Poelman, “A survey of augmented reality technologies, applications and limitations,” Int. J. Virtual Reality **9**, 1–20 (2010).

76. P. Milgram, H. Takemura, A. Utsumi, and F. Kishino “Augmented reality: a class of displays on the reality-virtuality continuum,” in Proc. SPIE **2351**, 282 (1995).

77. J. Carmigniani, B. Furht, M. Anisetti, P. Ceravolo, E. Damiani, and M. Ivkovic, “Augmented reality technologies, systems and applications,” Multimed. Tools Appl. **51**, 341-377 (2011).

78. J. Lee, A. Olwal, H. Ishii, and C. Boulanger, “SpaceTop: integrating 2D and spatial 3D interactions in a see-through desktop environment,” in SIGCHI Conference on Human Factors in Computing Systems (ACM, 2013), pp. 189-192.

79. H. Takahashi and S. Hirooka, “Stereoscopic see-through retinal projection head-mounted display,” Proc. SPIE **6803**, 68031N (2008).

80. H. Mukawa, K. Akutsu, I. Matsumura, and S. Nakano, “A full color eyewear display using holographic planar waveguides,” SID Symposium Digest of Technical Paper. **39**, 89–92 (2008).

81. Y. Takaki, Y. Urano, S. Kashiwada, H. Ando, and K. Nakamura, “Super multi-view windshield display for long-distance image information presentation,” Opt. Express **19**, 704-716 (2011).

82. J. Hong, S.-W. Min, and B. Lee, “Integral floating display systems for augmented reality,” Appl. Opt. **51**, 4201-4209 (2012).

83. J. Hong, Y. Kim, S.-g. Park, J.-H. Hong, S.-W. Min, S.-D. Lee, and B. Lee, “3D/2D convertible projection-type integral imaging using concave half mirror array,” Opt. Express **18**, 20628-20637 (2010).

84. K. Hong, J. Hong, J. Yeom, and B. Lee, “Two-dimensional and three-dimensional see-through screen using holographic optical elements,” in Biomedical Optics and 3-D Imaging, OSA Technical Digest (Optical Society of America, 2012), paper DM2C.6.

85. D. Fattal, Z. Peng, T. Tran, S. Vo, M. Fiorentino, J. Brug, and R. G. Beausoleil, “A multi-directional backlight for a wide-angle, glasses-free three-dimensional display,” Nature **495**, 348–351 (2013).

86. F. K. Bruder, F. Deuber, T. Fäcke, R. Hagen, D. Hönel, D. Jurbergs, T. Rölle, and M. S. Weiser, “Reaction diffusion model applied to high resolution Bayfol® HX photopolymer,” Proc. SPIE **7619**, 76190I (2010).

87. M. Ulibarrena, L. Carretero, R. Madrigal, S. Blaya, and A. Fimia, “Multiple band holographic reflection gratings recorded in new ultra-fine

grain emulsion BBVPan," Opt. Express **11**, 3385-3392 (2003).

88. J.-H. Park, K. Hong, and B. Lee, "Recent progress in three-dimensional information processing based on integral imaging," Appl. Opt. **48**, H77–H94 (2009).
89. Y. Kajiki, H. Yoshikawa, and T. Honda, "Hologram-like video images by 45-view stereoscopic display," Proc. SPIE **3012**, 154-166 (1997).
90. J.-H. Jung, K. Hong, and B. Lee, "Effect of viewing region satisfying super multi-view condition in integral imaging," SID Symposium Digest **43**, 883-886 (2012).
91. J. Hahn, Y. Kim, and B. Lee, "Uniform angular resolution integral imaging display with boundary folding mirrors," Appl. Opt. **48**, 504-511 (2009).
92. K. Hong, J. Hong, J. Yeom, and B. Lee, "Two-dimensional and three-dimensional see-through screen using holographic optical elements," in Biomedical Optics and 3-D Imaging, OSA Technical Digest (Optical Society of America, 2012), paper DM2C.6.
93. K. Hong, J. Yeom, and B. Lee, "Integral imaging using color multiplexed holographic optical element," in International Conference on 3D Imaging (IC3D) (IEEE, 2012), pp. 1-4.
94. K. Hong, J. Yeom, C. Jang, J. Hong, and B. Lee, "Full-color lens-array

holographic optical element for three-dimensional optical see-through augmented reality," Opt. Lett. **39**, 127-130 (2014).

95. M. K. Hedili, M. O. Freeman, and H. Urey, "Transmission characteristics of a bidirectional transparent screen based on reflective microlenses," Opt. Express **21**, 24636-24646. (2013).
96. R. Tasso, M. Sales, S. Chakmakjian, D. J. Schertler, and G. M. Morris, "LED illumination control and color mixing with engineered diffusers," Proc. SPIE **5530**, 133 (2004).
97. S. Chang, J. Yoon, H. Kim, J. Kim, B. Lee, and D. Shin, "Microlens array diffuser for a light-emitting diode backlight system," Opt. Lett. **31**, 3016-3018 (2006).
98. T.-W. Lin, C.-F. Chen, J.-J. Yang, and Y.-S. Liao, "A dual-directional light-control film with a high-sag and high-asymmetrical-shape microlens array fabricated by a UV imprinting process," J. Micromech. Microeng. **18**, 095029 (2008).
99. R. Bitterli, T. Scharf, H. Herzig, W. Noell, N. de Rooij, A. Bich, S. Roth, K. Weible, R. Voelkel, M. Zimmermann, and M. Schmidt, "Fabrication and characterization of linear diffusers based on concave micro lens arrays," Opt. Express **18**, 14251-14261 (2010).
100. M. K. Hedili, M. O. Freeman, and H. Urey, "Microlens array-based

high-gain screen design for direct projection head-up displays," Appl. Opt. **52**, 1351-1357 (2013).

101. M. Okui, J. Arai, Y. Nojiri, and F. Okano, "Optical screen for direct projection of integral imaging," Appl. Opt. **45**, 9132-9139 (2006).

102. R. Martínez-Cuenca, H. Navarro, G. Saavedra, B. Javidi, and M. Martinez-Corral, "Enhanced viewing-angle integral imaging by multiple-axis telecentric relay system," Opt. Express **15**, 16255-16260 (2007).

103. S. Park, B. Song, and S. Min, "Analysis of image visibility in projection-type integral imaging system without diffuser," J. Opt. Soc. Korea **14**, 121-126 (2010).

104. Grapac Japan. http://www.grapac.co.jp/eng_hals/index.html

105. Fresneltech. http://www.fresneltech.com/

Appendix

Portions of the work discussed in this dissertation are also presented in the following publications:

[Chapter 3] K. Hong, S.-g. Park, J. Yeom, J. Kim, N. Chen, K. Pyun, C. Choi, S. Kim, J. An, H.-S. Lee, U-in. Chung, and B. Lee, "Resolution enhancement of holographic printer using a hogel overlapping method," Opt. Express **21**, 14047-14055 (2013).

[Chapter 4.2] K. Hong, J. Yeom, C. Jang, G. Li, J. Hong, and B. Lee, "Two-dimensional and three-dimensional transparent screens based on lens-array holographic optical elements," Opt. Express **22**, 14363-14374 (2014).

[Chapter 4.3] K. Hong, J. Yeom, C. Jang, J. Hong, and B. Lee, "Full-color lens-array holographic optical element for three-dimensional optical see-through augmented reality," Opt. Lett. **39**, 127-130 (2014).

초 록

이 박사학위 논문에서는 새로운 홀로그래픽 기록방법들을 이용하여 기존의 무안경식 삼차원 디스플레이의 제한점들을 개선하는 방법에 대해 논한다. 두 종류의 새로운 홀로그래픽 기록방법을 무안경식 삼차원 디스플레이를 구현하기 위해 제안한다. 첫 번째 방법은 호겔 중첩을 이용하여 홀로그래픽 스테레오그램의 해상도를 증가시키는 방법이며, 다른 하나의 방법은 렌즈어레이 홀로그래픽 광학소자를 이용하여 투명한 특성을 가지는 이차원 및 삼차원 영상을 구현하는 방법이다.

이 박사학위 논문에서는 홀로그래픽 기록매질로 광중합체 필름을 사용한다. 단일파장 기록방법과 세 파장 다중화 기록방법을 이용해 제작된 광중합체 필름 상에 기록되는 체적홀로그램에 대한 노출반응 특성을 실험을 통해 분석한다. 광중합체 필름에 기록된 세 파장 다중화된 홀로그램의 투명한 특성과 회절효율을 재생실험을 통해 평가하며, 광중합체 필름의 수축특성에 대해 이론적으로 분석하고 실험적으로 검증한다.

홀로그래픽 프린팅 방법을 이용해 기록된 홀로그래픽 스테레오그램의 해상도를 증가시키기 위한 호겔중첩 방법을 제안한다. 홀로그래픽 프린팅 방법을 이용해 홀로그래픽

스테레오그램을 기록할 때 해상도 증가를 위해 호겔의 크기를 무한정 줄일 수 없음을 컴퓨터 시뮬레이션을 통해 검증한다. 호겔 크기를 줄여 해상도를 증가시키는 방법 대신에 호겔을 중첩 기록시키는 방법을 이용해 홀로그래픽 스테레오그램의 해상도를 증가시킬 수 있는 방법을 제안한다. 홀로그래픽 스테레오그램을 기록할 수 있는 실험환경을 구축하였으며 이를 이용하여 기존의 방법과 제안된 호겔 중첩 방법을 적용한 서로 다른 두 개의 홀로그래픽 스테레오그램을 제작한다. 제작된 두 개의 홀로그래픽 스테레오그램의 재생 영상을 비교함으로써 제안된 호겔중첩 방법을 적용한 홀로그래픽 스테레오그램이 기존의 방법보다 높은 해상도를 가짐을 검증한다.

집적영상을 통해 투명한 특성을 가지는 이차원 및 삼차원 가상영상을 재생할 수 있는 렌즈어레이 홀로그래픽 광학소자를 제안한다. 홀로그래픽 광학소자를 기록하기 위한 실험환경에 파장다중화 기록 방법과 공간다중화 기록방법을 적용하여 총천연색 홀로그램 기록과 대면적 기록을 가능하게 하는 방법에 대해 논한다. 제안된 렌즈어레이 홀로그래픽 광학소자의 특성을 재생실험을 통해 평가한다. 제안된 구조에서 재생된 집적영상을 통해 렌즈어레이 홀로그래픽 광학소자가 증강현실 기술에 적용하기 적합한 광학적으로 투명한 특성을 만족시키면서 총천연색의 삼차원

가상영상을 재생 가능함을 검증한다. 제안된 렌즈어레이 홀로그래픽 광학소자를 통해 재생되는 영상의 관찰특성들을 렌즈어레이 홀로그래픽 광학소자의 광학변수들을 이용하여 평가하며, 이를 이용해 제안된 방법이 이차원/삼차원 투명스크린으로 사용될 수 있는 가능성을 제시한다. 이차원과 삼차원 투명스크린 역할을 할 수 있는 두 개의 서로 다른 사양의 렌즈어레이 홀로그래픽 광학소자들을 제작한다. 이 두 렌즈어레이 홀로그래픽 광학소자들은 재생실험의 결과를 통해 이차원/삼차원 투명 스크린으로 응용할 수 있음을 보이며, 이 때 재생되는 영상들의 관찰 특성들을 평가한다. 또한 외부의 이미지 프로젝터 등의 광변조장치를 통해 제공되는 영상정보를 사용하여 렌즈어레이 홀로그래픽 광학소자 상에서 동적 삼차원 가상영상을 재생하는 방법을 제시한다. 동적 요소영상을 컴퓨터 그래픽스를 이용하여 제작하였으며, 제안된 렌즈어레이 홀로그래픽 광학소자가 동적 삼차원 가상영상을 재생할 수 있음을 실험적으로 검증한다.

주요어: 무안경식 삼차원 디스플레이, 홀로그래픽 프린팅, 홀로그래픽 광학소자, 체적 홀로그램, 집적영상, 포토폴리머.

학 번: 2008-21006